REPUBLIC OF TURKEY

ADANA ALPARSLAN TÜRKEŞ SCIENCE AND TECHNOLOGY UNIVERSITY

GRADUATE SCHOOL OF NATURAL AND APPLIED SCIENCES DEPARTMENT OF MATERIALS SCIENCE AND ENGINEERING

PREPARATION OF ZIF-8/TiO_2 NANO-COMPOSITE THIN FILMS FOR SOLAR ENERGY APPLICATIONS

ONUR İLOĞLU

MASTER OF SCIENCE

ADANA 2022

REPUBLIC OF TURKEY

ADANA ALPARSLAN TÜRKEŞ SCIENCE AND TECHNOLOGY UNIVERSITY

GRADUATE SCHOOL OF NATURAL AND APPLIED SCIENCES DEPARTMENT OF MATERIALS SCIENCE AND ENGINEERING

PREPARATION OF ZIF-8/TiO_2 NANO-COMPOSITE THIN FILMS FOR SOLAR ENERGY APPLICATIONS

ONUR İLOĞLU
MASTER OF SCIENCE

SUPERVISOR

ASST. PROF. DR. Hüsnü Arda YURTSEVER

ADANA 2022

I hereby declare that all information in this thesis has been obtained and presented in accordance with academic rules and ethical conduct. I also declare that, as required by these rules and conduct, I have fully cited and referenced all information that is not original to this work.

Onur İLOĞLU

ABSTRACT

PREPARATION OF ZIF-8/TiO_2 NANO-COMPOSITE THIN FILMS FOR SOLAR ENERGY APPLICATIONS

Onur İLOĞLU

Department of Materials

Science and Engineering

Supervisor: Asst. Prof. Hüsnü Arda YURTSEVER

March 2022, 66 pages

Excessive use of fossil fuels due to the constantly growing energy demand of mankind causes global warming which will be irreversible soon if fossil fuels are not replaced with renewable and green energy sources. Photocatalysis is expected to be a solution to global warming by which hydrogen can be produced by water splitting or renewable fuels such as methanol, ethanol or formic acid can be produced by photoreduction of carbon dioxide. Design and production of photocatalytic materials play a central role in the efficiency and feasibility of a photocatalytic process.

The aim of this study is to design and prepare active photocatalytic thin films based on titanium dioxide (TiO_2) and zeolitic imidazolate framework-8 (ZIF-8) and determine their activities in photocatalytic applications. The desired properties of TiO_2 as a highly efficient photocatalyst and microporous structure of ZIF-8 which makes it a promising material in the use of gas involving processes such as hydrogen storage and gas separation are the main reasons for choosing them as the constitents of a composite photocatalytic material. These properties would provide the desired properties that will make the photocatalyst have high activities in water splitting and carbon dioxide reduction reactions.

In this study, nanocomposite thin films were prepared in two different forms, transparent and particulate thin films, by a simple dip coating method. In the first part, the optimum heat treatment temperature and the optimum number of layers were initially determined for the preparation of TiO_2 layer. ZIF-8 was next grown on TiO_2 layer and optimum crystal formation time and zinc/methylimidazole ratios were determined for ZIF-8 growth. In order to increase the photocatalytic performance of ZIF-8/TiO_2 composite thin films, copper, cerium, zinc and iron doped TiO_2 films were also synthesized and their performances were evaluated. Photocatalytic performances of these films were determined by methylene blue degradation which is an easier, fast and cheaper photocatalytic activity determination method compared to water splitting and carbon dioxide reduction. Photocatalytic performance determination experiments showed that the highest photocatalytic activities of ZIF-8/TiO_2 films were obtained with the films prepared by using 1 % cerium, zinc, iron or copper doped TiO_2 films.

In the second part, particulate thin films were prepared by using previously synthesized ZIF-8, a commercial TiO_2 powder Degussa P25 and titanium precursor (titanium tetraisopropoxide). In this part, the optimum number of layers and heat treatment temperature were determined. The relation between the photocatalytic activity and structural properties was revealed by characterization techniques such as X-ray Photoelectron Spectroscopy, X-ray Diffraction, UV-Vis Spectroscopy and Scanning Electron Microscopy throughout these studies. The highest activity (78 %) was obtained with the particulate thin film heat treated at 500˚C having 5 layers of ZIF-8/P25/TiO_2 composite structure. The characterization studies indicated that ZIF-8 was oxidized and N doped TiO_2 or ZnO structure was formed. The band gap of this film was also found to be very low (2.14 eV) compared to those of other films which indicated that this film absorbs light more efficiently than the other films. Silver doped ZIF-8 was also synthesized to prepare an Ag-ZIF-8/P25/TiO_2 composite thin film and the efficiency of this film was determined to be 72 % which was lower than ZIF-8/P25/TiO_2.

Keywords: solar energy, photocatalysis, thin film, TiO_2, ZIF-8

ÖZET

GÜNEŞ ENERJİSİ UYGULAMALARINA YÖNELİK ZIF-8/TiO_2 NANO-KOMPOZİT İNCE FİLMLERİN ÜRETİMİ

Onur İLOĞLU
Malzeme Bilimi ve
Mühendisliği Anabilim
Dalı
Danışman: Dr. Öğr. Üyesi Hüsnü Arda
YURTSEVER
Mart 2022, 66 sayfa

İnsanlığın sürekli artan enerji talebi nedeniyle fosil yakıtların aşırı kullanımı, fosil yakıtların yerini yenilenebilir ve yeşil enerji kaynaklarına bırakmadığı takdirde kısa sürede geri dönüşü olmayan küresel ısınmaya neden olacaktır. Suyun parçalanmasıyla hidrojen eldesini, karbondioksitin fotoindirgemesiyle metanol, etanol veya formik asit gibi yenilenebilir yakıtların üretilebilmesini sağlayan fotokatalizin küresel ısınmaya bir çözüm olması beklenmektedir. Fotokatalitik malzemelerin tasarımı ve üretimi, bir fotokatalitik işlemin verimliliğinde ve uygulanabilirliğinde merkezi bir rol oynamaktadır.

Bu çalışmanın amacı titanyum dioksit (TiO_2) ve zeolitik imidazolat kafes-8 (ZIF-8) bazlı aktif fotokatalitik ince filmler tasarlamak, üretmek ve fotokatalitik uygulamalardaki etkinliklerini belirlemektir. TiO_2'in yüksek verimli bir fotokatalizör olarak istenen özelliklere sahip olması ve hidrojen depolama ve gaz ayrımı gibi gazları içeren uygulamalarda kullanımını sağlayan ZIF-8'in mikro gözenekli yapısının olması gibi nedenlerle bu iki malzeme kompozit bir fotokatalitik yapı oluşturulması için seçilmiştir. Bu özellikler, fotokatalizörün su ayırma ve

karbondioksit indirgeme reaksiyonlarında yüksek aktivitelere sahip olmasını sağlayacak gerekli özelliklerdir.

Bu çalışmada, nanokompozit ince filmler, basit bir daldırma kaplama yöntemi ile şeffaf ince filmler ve partiküler ince filmler olmak üzere iki farklı yapıda üretilmiştir. Birinci bölümde öncelikle TiO_2 tabakası için optimum ısıl işlem sıcaklığı ve optimum tabaka sayısı belirlenmiştir. Bir sonraki aşamada, TiO_2 tabakası üzerinde ZIF-8 büyütülmüş ve ZIF-8 büyümesi için optimum kristal oluşum süresi ve çinko/metilimidazol oranları belirlenmiştir. ZIF-8/TiO_2 kompozit ince filmlerin fotokatalitik performansını artırmak için ayrıca bakır, seryum, çinko ve demir katkılı TiO_2 filmleri de sentezlenmiş ve performansları belirlenmiştir. Bu filmlerin fotokatalitik performansları, su parçalama ve karbondioksit indirgeme ile karşılaştırıldığında daha kolay, hızlı ve daha ucuz bir fotokatalitik aktivite belirleme yöntemi olan metilen mavisi bozundurması ile belirlenmiştir. Fotokatalitik performans belirleme deneyleri, ZIF-8/TiO_2 filmlerinin en yüksek fotokatalitik aktivitelerinin % 1 seryum, çinko, demir veya bakır katkılı TiO_2 filmlerle hazırlanan filmlerle elde edildiğini göstermiştir.

İkinci bölümde, partiküler ince filmler daha önce sentezlenen ZIF-8, ticari TiO_2 tozu Degussa P25 ve titanyum öncülü (titanyum izopropoksit) kullanılarak sentezlenmiştir. Bu bölümde optimum tabaka sayısı ve ısıl işlem sıcaklığı belirlenmiştir. X-ışını Fotoelektron Spektroskopisi, X-ışını Kırınımı, UV-Vis Spektroskopisi ve Taramalı Elektron Mikroskobu gibi karakterizasyon teknikleri ile yapısal özellikler ve fotokatalitik aktivite arasındaki ilişki bu çalışmalarla ortaya konmuştur. En yüksek aktivite (% 78), 5 katmanlı ZIF-8/P25/TiO_2 kompozit yapıya sahip 500˚C'de ısıl işlem görmüş partiküler ince film ile elde edilmiştir. Karakterizasyon çalışmaları, ZIF-8'in oksitlendiğini ve N katkılı TiO_2 veya ZnO yapısının elde edildiğini göstermiştir. Bu filmin bant genişiliğinin de diğer filmlere kıyasla çok düşük (2,14 eV) olduğu bulunmuştur, bu da bu filmin ışığı diğer filmlerden daha verimli bir şekilde soğurduğunu göstermektedir. Ayrıca, Ag-ZIF-8/P25/TiO_2 kompozit ince film hazırlamak için gümüş katkılı ZIF-8 de sentezlenmiş ve bu filmin veriminin ZIF-8/P25/TiO_2'den daha düşük (% 72) olduğu belirlenmiştir.

Anahtar Kelimeler: güneş enerjisi, fotokataliz, ince film, TiO_2, ZIF-8

ACKNOWLEDGEMENTS

I would like to express my deepest gratitude to my advisor, Asst. Prof. Dr. Hüsnü Arda Yurtsever, who shared his knowledge and experience with me throughout my thesis, helped me develop theoretically and experimentally and supported and encouraged me from the beginning to the end of the project.

I would like to thank my thesis committee members Asst. Prof. Dr. Ali Emrah ÇETİN and Asst. Prof. Dr. Burcu ALP for their ideas and feedback.

I would like to thank the Food Engineering Department of Alparslan Türkeş Science and Technology University, which provided me with the opportunity to carry out the performance determination studies in my thesis.

Also, I would like to thank my laboratory mates Kubilay Erzin, Serkan Saday, Arif Karakuş for their help and support.

Thanks to THE SCIENTIFIC AND TECHNOLOGICAL RESEARCH COUNCIL OF TURKEY (TÜBİTAK) for awarding me a National Scholarship in Priority Fields in Science-2210/C Fellowship, providing me with the financial means to complete this thesis.

This thesis was financially supported by the ALPARSLAN TÜRKEŞ SCIENCE AND TECHNOLOGY UNIVERSITY Scientific Research Coordination Unit with the project numbers of 20303001 and 19103015.

TABLE OF CONTENTS

LIST OF FIGURES

LIST OF TABLES

1. INTRODUCTION

The energy demand of mankind is increasing day by day and this energy demand is generally met by fossil fuels and nuclear energy. 85% of global energy is dependent on fossil fuels. Fossil fuel dependency of leading countries are; China 87%, U.S. 85.3%, the EU 75.4%, India 92.5%, Russia 87.1% and Japan 90.8%. Fossil fuel reserves of all world are 839.7 billion-tones-of-oil-equivalent (btoe), 51.4% of that is coal, 28.6% is oil, 20.0% belongs to natural gas and their average reserves-to-production ratio (R/P) is 93.5 yr. in comparison to coal (152.7 yr.), gas (52.5 yr.) and oil (50.7 yr.) (Ediger, 2019).

The use of both energy sources have negative effects on the environment and human health. The gases generated as a result of the burning of fossil fuels (SO_x, NO_x, CO_x) seriously affect the environment and human health and global warming, which is the consequence of fossil fuel burning, has increased from past to present. Global warming can be defined as the rise in the average surface temperature of the world (Al-Ghussain, 2019). The first estimate about global surface temperature (carbonic acid concentration effect on global surface temperature) was made by Swedish chemist Svante Arrhenius more than one hundred years ago. After the first estimates and following studies, global warming has become the subject of debate in the media, public and political arena mid to late the 1980s (Khandekar et al., 2005). Global warming causes unavoidable climate change. Prevention of climate change caused by global warming will be possible by turning to clean energy resources. Renewable energy sources can satisfy the energy demand of the world and due to these properties, renewable energy sources have huge potential. Bioenergy, wind, solar, hydropower and geothermal energy sources are used as harmless renewable sources (Antonia et al., 2001; Owusu et al., 2016).

Solar energy is an energy type of which utilizes the radiant light and heat of the sun. In a solar energy application, collected light or heat of the sun is converted to electrical or thermal energy. Non-toxicity, environmentally friendliness, ability to reduce carbon print and being an endless source make solar energy the most promising source compared to other types of renewable energy sources. Solar panels, solar ponds, molten salt towers and photocatalysis are different application areas solar energy.

Fossil fuel consumption rise to satisfy the needs of the growing population and the increasing energy demand, caused massive release of hazardeous gases like CO_x, NO_x and SO_x from power plants, industry and transportation to the atmosphere which directly affect the environment and human health. Air pollution, water pollution, viral and bacterial diseases and global warming are among the factors that affect the environment and human health. Photocatalysis can be used to reduce the amounts of hazardeous gases in the atmosphere and to produce renewable and green energy sources like hydrogen and methanol. Photocatalysis is a type of catalaytic reaction in which solar light activates a photocatalyst and various oxidation-reduction reactions are triggered by the activated photocatalyst. These phototriggered reactions can reduce the energy need to start an oxidation or reduction reaction in which reactants are converted to desired products at atmospheric conditions. Thus, photocatalysis may eventually reduce the need for fossil fuels by producing green energy sources, inactivate bacteria and viruses and help reduce water/air pollution by oxidizing pollutants.

The main purpose of this thesis is to design and prepare a double layer composite structures consisting of TiO_2 and ZIF-8 and to determine their potential use in solar energy applications. The main reasons of choosing TiO_2 and ZIF-8 are that TiO_2 is chemically/photochemically inert, inexpensive and it is easy to modify the properties which directly affect the photocatalytic activity such as band gap energy and crystalline structure whereas ZIF-8 has the ability to adsorb CO_2 which is a greenhouse gas that cause global warming. Thus the main idea is to design a photocatalyst which has potential use in solar energy applications such as artifical photosynthesis and green energy production. The determination of activity in artificial photosytnhesis reactions and the quantification of reaction products need complicated experimentation and equipment, that is why the activities of the prepared composites were determined in the photocatalytic oxidation of textile dyes which is relatively less complicated.

In this thesis, iron (Fe), copper (Cu), cerium (Ce) or zinc (Zn) doped TiO_2 layers were produced as the first layer and ZIF-8 was grown as the second layer of the ZIF-8/TiO2 photocatalyst films. This thesis can be divided into two parts:

- The first part contains the results of characterization and activity determination experiments of ZIF-8/TiO_2 transparent composite thin films. In this part, the effects of heat treatment temperature, number of layers, type and amounts of dopants on the photocatalytic activity were investigated. After determination of the optimum parameters (heat treatment temperature, number of layers, dopant type and dopant amount) for the TiO_2 layer, the effects of ZIF-8 crystal growth time and the ratio of zinc and methyl imidazole on the properties and photocatalytic activities of the films were investigated.

- The second part contains the results of characterization and activity determination experiments with the films which were prepared by using constituent materials (TiO_2 and ZIF-8) in particulate form. Firstly, ZIF-8 was synthesized and then used in the preparation of thin films. These films contain ZIF-8, Degussa P25 (a commercial TiO_2 powder) and a laboratory-synthesized TiO_2. Thus, these films can be denoted by ZIF-8/P25/TiO_2. The effects of heat treatment temperature and the number of layers on the properties and photocatalytic activities of the films were investigated in this part.

2. LITERATURE REVIEW

2.1. Renewable Energy Sources

Renewable energy can be defined as the energy which is obtained from a natural source that can constantly be replenished. Renewable energy sources are divided into five main groups according to their source types. These sources are biomass, wind, water, geothermal and solar.

2.1.1. Bioenergy

Bioenergy is obtained by anaerobic decomposition of wastes of trees, crops and organic materials obtained from plants. The source which is required for bioenergy is called biomass. Biomass is obtained directly from the soil, the residue of the wood industry, food, and paper. Biomass energy can be converted into a useful form such as heat energy, electricity and liquid fuel. Today, 40-55 EJ (EJ=10^{18}) biomass is used for energy generation, this value is equal to 10-14% of total energy generation and it makes it the fourth largest energy source after oil (33%), coal (21%) natural gas (19%) (Antonia, 2001).

2.1.2. Wind Energy

Wind energy is obtained from the conversion of the kinetic energy of air to electrical energy through wind turbines. Wind energy history is based on windmills which are used in China, India, Persia from 2000 years ago. The potential of wind energy is estimated to be 26,000 TWh/yr, although it is used with 9000 TWh/yr capacity because of economical and other reasons (Antonia et al., 2001; Panwara et al., 2011).

2.1.3. Hydropower Energy

Hydropower energy is the biggest renewable energy source for producing electricity and it is used by more than 150 countries worldwide. Hydropower energy is obtained by the conversion of kinetic energy of water. When water flows from a higher level to a lower level, the kinetic energy of water is converted to electrical energy through turbines and generators in powerplants. The annual energy potential of hydropower energy is 14,576 TWh and conjectural total potential is 3.721 GW, but at present less capacity is used compared to its potential (Owusu et al., 2016).

2.1.4. Geothermal Energy

For thousands of years, people utilize hot springs and steam vents for providing daily needs (bathing, cooking and heating). Geothermal energy has been used for more than 70 years directly (for space heating, aquaculture and industrial process) or indirectly for obtaining electricity. Geothermal energy is obtained from the drilling of hydrothermal reservoirs in earth's crust, steam and hot water are transported to the surface by pipes. Then it can be used directly or turned to electricity. Electricity producing capacity and direct use capacity of geothermal energy is 12,000 TWh/year and 600,000 EJ, respectively. But this potential is not used with 100% capacity. 44,000 TWh/year amount is used for producing electricity and 38.000 TWh/year is used for direct use (Antonia et al., 2001; Owusu et al., 2016).

2.1.5. Solar Energy

Solar energy is the collecting of sunlight with reflectors and absorber surfaces and conversion to electricity or heat. The energy amount that comes from the sun to the earth's surface is 120 petawatts, (1 petawatt= 10^{15} watt), which means that energy obtained from the sun in a day provides the world's energy demand for more than 20 years (Chu, 2011). Energy consumption of the world is 16 TWy/year while 23,000 TWy/year energy can be obtained from the sun. A schematic comparison of the potentials of the renewable and non-renewable energy sources are given in Figure 2.1.

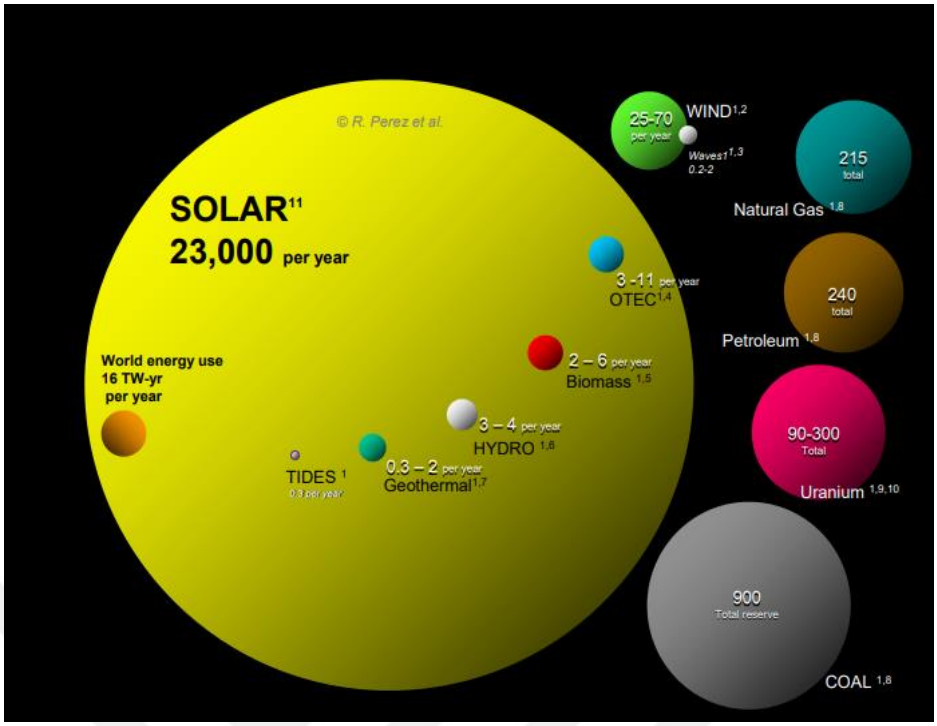

Figure 2.1. Comparison of the energy amount of various sources (Richard Perez & Marc Perez 2009)

Different types of methods are used for solar energy conversion, the most common one is the collection of sunlight which is focused by the panels and reflectors. Sunlight can be redirected or is collected as heat to provide power to the turbine and heat engine (Barlev et al., 2011).

Solar panels, solar ponds, solar towers and photocatalysis are different ways of solar energy conversion. Solar panels are used to convert solar energy to electricity. Semiconductor materials are used in solar panels which are connected solar cells. These materials are capable of collecting sunlight and converting it to direct current (DC) (Rizk & Chaiko 2008).

Solar pond is a pool filled with water that has variable salt concentration (salt concentration of water increases towards the bottom). The layer that has high salt concentration is heated more by sunlight and the obtained heat can be used for heating, drying, desalination or in a turbine to produce electricity (Panchal et al., 2020).

Solar towers are another electricity generator technology from sunlight. Sunlight is reflected from to receiver which is placed at top of the tower with mirrors. The receiver is fed with cold salt, salt absorbs the sunlight and the heat of salt increases. Hot salt is forwarded into the

steam generator and steam operates the turbine and electricity is produced (Benramdane et al., 2019).

Photocatalysis is a catalytic process in which photocatalysts utilize solar light to trigger oxidation-reduction reactions. Photocatalyst working mechanism is based on semiconductor working mechanism. Excited valance band electrons through light energy go to conduction band and reactions occur (reduction and oxidation reactions) in valance and conduction bands (Hall, 1991).

2.1 Photocatalysis

Photocatalysis word is the combination of ''photo'' (means light) and ''catalysis'' (means break apart or decompose) (Ameta, 2016). Photocatalysis is a catalytic reaction that begins with the absorption of light by a catalyst and involves the conversion of a substrate into products (Houk, 1988). Photocatalysis is divided into two parts; homogenous and heterogeneous photocatalysis. If reactant and photocatalyst have the same phase photocatalysis is called homogenous whereas, if reactant and photocatalyst have different phases photocatalysis is called heterogeneous photocatalysis.

2.2.1. Working Principle of a Photocatalyst

Photocatalysts are semiconductor-based materials therefore photocatalyst working mechanism is based on the semiconductor working mechanism. Electron is excited by light, electron energy is increased, the electron which is on the valance band exceeds the bandgap energy and goes through conduction band and conductivity occurs. A schematic of the semiconductor working mechanism is shown in Figure 2.2 The behavior of the semiconductor is dominated by electrons close to the top of the valence band and to the bottom of the conduction band, where the energy distribution relations ε(k);

Conduction band: $\varepsilon = E_G + \frac{h^2k^2}{me}$ (2.1)

Valance band: $\varepsilon = -\frac{h^2k^2}{mh}$ (2.2)

where, ε is energy, E_G is band gap energy, h is Planck's constant, k is wavevector, me is free particle positive mass and mh is negative effective mass.

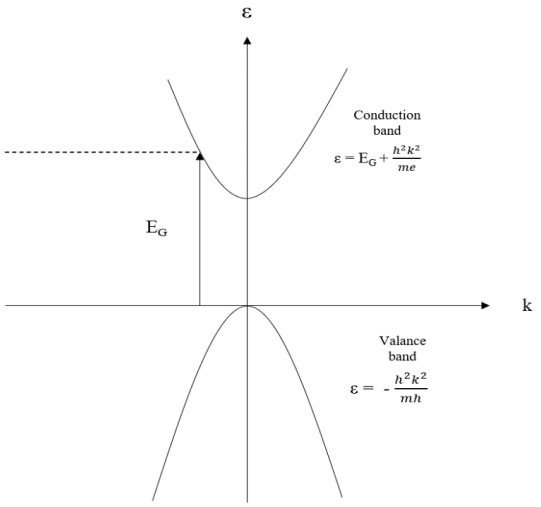

Figure 2.2. A schematic of semiconductor working mechanism (Hall, 1991)

Conductivity and structure affect the performance of the photocatalyst. Conductivity is generally increased by thermal excitation of carriers, intrinsic behavior, and extrinsic behavior (Hall, 1991). These properties can be provided through doping. With the addition of the dopants, the bandgap of the photocatalyst becomes narrower, oxygen vacancies occur, crystallinity, optical properties, surface morphology, surface area, porosity, and wettability change. Doping types for a semiconductor photocatalyst are metal doping, non-metal doping, and co-doping. Metal doping is created with different types of metals such as copper, vanadium, cobalt, zinc, iron, etc. Most metal oxides have restricted light absorption and inadequate charge separation but the metal used as the dopant improves the morphology, electronic, magnetic and photocatalytic properties through redox potential utilization by the expansion of absorption range in the visible region. Non-metals such as C, S, F, Si, P and Br can be used as dopants. Non-metal doping decreases the bandgap energy, increases electron trapping, and hence increases photocatalytic activity. Another doping type is co-doping. Co-doping is the addition of donor-acceptor to semiconductors with metal-metal, metal-nonmetal, nonmetal-nonmetal elements. The addition of different types of donor-acceptor decreases bandgap energy and shifts the absorption edge from the UV region to the visible region. The main purpose of co-doping is to decrease charge carrier recombination rate and to increase carrier mobility (Ameta & S. Ameta 2016).

2.2.2. Application Areas of Photocatalysis

Photocatalysis is a cost-efficient and environmentally friendly method which can be used in environmental and energy-related applications such as wastewater treatment, air cleaning, virus and bacteria inactivation and hydrogen production.

2.2.2.1. Wastewater Treatment

Wastewater treatment is based on the photocatalytic oxidation of contaminant molecules in wastewater from the textile or pharmaceutical industry. Photocatalytic oxidation is briefly explained as the formation of vacancies and electrons in the semiconductor material formed upon excitation by light. Valence band electrons (e^-) excited by appropriate energy move to the conduction band and form a hole (h^+) in the valence band. Oxidation in the valence band and reduction in the conduction band take place due to the charge carriers moving to the material surface and material interface. As a result of the oxidation/reduction reactions, superoxide radicals ($O_2^{\cdot}$) and hydroxyl groups ($HO^{-\cdot}$, $HO_2^{\cdot -}$), which are reactive oxygen species (ROS), are formed and oxidize the organic contaminant (Dalrymple et al., 2010; Foster et al., 2011; Gerrity et al., 2008; Laxma et al., 2017; Nakano et al., 2012; Zhang et al., 2019). A schematic representation for the oxidation reactions occurring on a photocatalyst is shown in Figure 2.3.

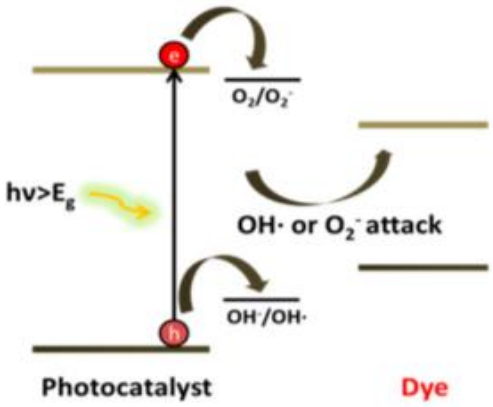

Figure 2.3. A schematic representation for the oxidation reactions occurring on a photocatalyst (Rochkind, 2014)

2.2.2.2 Air Cleaning

Photocatalytic air cleaning is the decomposition of organic pollutants (benzene, toluene etc.) into harmless CO_2 and other inorganic species or conversion of inorganic pollutants (NO, CO) to harmless molecules such as CO_2 and N_2. Electrons and holes that are formed upon excitation oxidize/reduce organic/inorganic pollutants, which were adsorbed from the gas phase, to harmless species (Ren et al., 2017). A schematic representation of the pollutant removal by photocatalysis is given in Figure 2.4.

Degradation of pollutants:

1. Direct Redox

   e^-/h^+ —(pollutants)→ Inorganic Products

2. Radical formation and Redox

   e^-/h^+ —(O_2/H_2O)→ Radicals

3. Radical Formation, ROS formation, and redox

   e^-/h^+ —(O_2/H_2O)→ Radicals → ROS —(pollutants)→ Inorganic Product

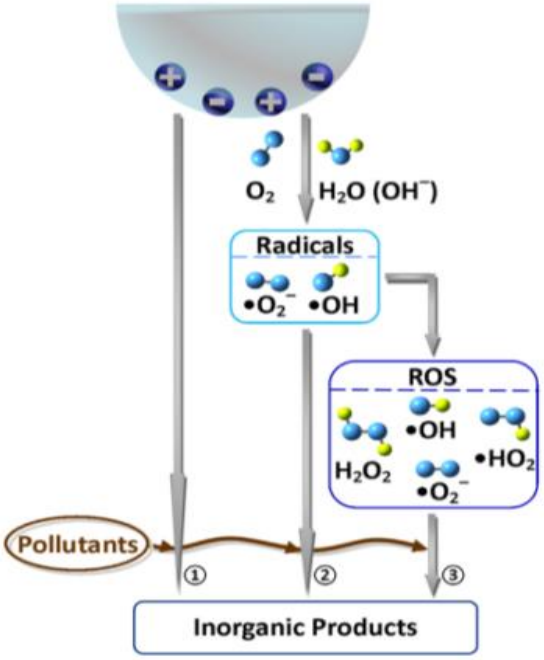

Figure 2.4. A schematic representation of the pollutant removal by photocatalysis (Ren et al., 2017)

2.2.2.3. Virus and Bacteria Inactivation

Photocatalysts eliminate viruses and bacteria through attacking of ROS to cell membrane. With the help of high oxidative properties of photocatalysts, the formed superoxide radicals and hydroxyl groups attack virus capsids, virus binding sites, DNA, amino acids and organic components in their structure and hence viruses/bacteria become inactivated (Dalrymple et al., 2010; Foster et al., 2011; Gerrity et al., 2008; Laxma et al., 2017; Nakano et al., 2012; Rincón & Pulgarin, 2004; Zhang et al., 2019). A schematic representation of photocatalytic inactivation of bacteria is given in Figure 2.5.

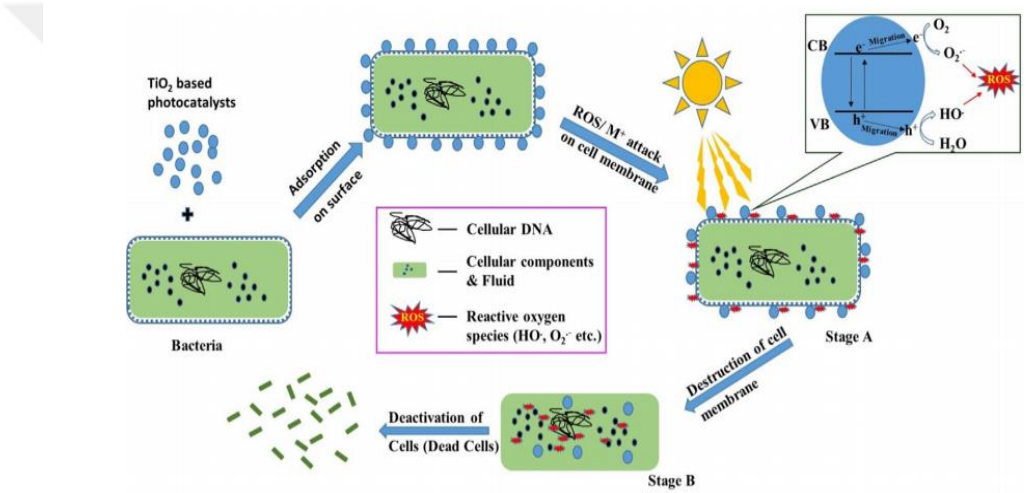

Figure 2.5. Photocatalytic inactivation of bacteria (Laxma et al., 2017)

2.2.2.4. Photocatalytic Hydrogen Production

Photocatalytic hydrogen production is currently and mostly studied due to hydrogen's being a cleaner energy source compared to fossil fuels. It's realized by water splitting which produces H_2 and O_2. As the general photocatalysis mechanism, with the excitation of electrons on the valance band under appropriate light, excited electrons go through the conduction band and holes are formed on the valance band. Positively charged particles are accepted by H_2O and H_2O is converted to $2H^+$ and O_2 through oxidation whereas on the conduction band, $2H^+$ species accept electrons and are reduced to H_2 (Ni et al., 2007; Shi et al., 2019). A schematic representation of photocatalytic hydrogen production mechanism is given in Figure 2.6.

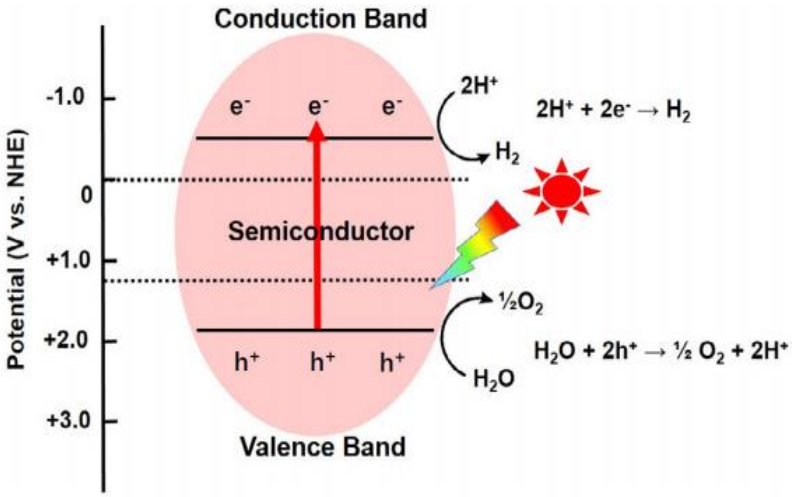

Figure 2.6. A schematic representation of photocatalytic hydrogen production mechanism (Shi et al., 2019)

2.2.3. Photocatalytic Materials

Photocatalysts are semiconductor materials that are mostly oxides, nitrides, and phosphides (Di Paola et al.,2012; Sun et al., 2020). Metal oxide materials are commonly used as photocatalysts due to their thermal/photochemical stability, environmental friendliness, and cost-effectiveness. TiO_2, ZnO, WO_3, Fe_2O_3, C_3N_4 are the most common ones and some properties of these materials are given below.

Zinc oxide (ZnO) is a widely preferred photocatalyst due to its low cost and high performance in the wastewater treatment process (Di Paola et al., 2012; Sun et al., 2020). ZnO is not harmful to the environment and the human body. Due to its limited band gap and its easy dissolution at extreme pH levels, zinc oxide restricts its use in some photocatalytic applications (Di Paola et al., 2012; Sun et al., 2020). The photocatalytic efficiency of ZnO can be enhanced by surface modification, morphological alteration, and doping (Sun et al., 2020; Zhou et al., 2016). WO_3 is an n-type semiconductor material that works under visible light due to its lower band gap (E_G= 2.4-2.8 eV) (Sun et al., 2020). WO_3 is used in bacterial disinfection, heavy metal removal, and gas sensing applications. Pollutant degradation properties of WO_3 are high due to its low charge carrier recombination rate (Di Paola et al., 2012). The ease of enhancement of photocatalytic activity by morphology tuning, surface

modification, doping with transition and non-transition metals, and photochemical stability make WO_3 a commonly used material in photocatalytic applications (Di Paola et al., 2012; Sun et al., 2020).

Fe_2O_3 is a narrow band gap (E_G=1.9-2.2 eV) semiconductor material that is used in many photocatalytic applications (Sun et al., 2020). Fe_2O_3 is generally used in gas sensing, degradation of dyes and degradation of various hydrocarbons (Di Paola et al., 2012; Sun et al., 2020). Its low electron/hole recombination rate, chemical stability, low cost, non-toxicity, and ease of enhancement in its activity make it popular for photocatalytic applications (Di Paola et al., 2012; Sun et al., 2020).

Carbon nitride is a semiconductor that is formed with C and N atoms and it is a synthetic material. Its band gap is 2.7 eV. C_3N_4 is especially used with graphite for the enhancement of its photocatalytic performance (Zhou et al., 2016). Although it is not found naturally, the widespread availability of carbon and nitrogen makes it cost-effective to produce. In addition to this property, due to its resistance to acid, high corrosion resistance, and high absorption capacity of visible light, carbon nitride is an important material for photocatalytic applications (Sun et al., 2020; Zhou et al., 2016).

2.2.3.1. Titanium Dioxide (TiO_2)

TiO_2 is the most common material used in catalytic and photocatalytic applications such as CO oxidation, deoxygenation, hydrogeneration, self-cleaning and antimicrobial applications, gas sensorsdue to its non-toxicity, cost-effectiveness, long-term stability, suitable conduction, and valance band positions (Hashimoto et al., 2005; Oi et al., 2016; Zhang et al., 2014). Also, TiO_2 is used in paint, fillers in the paper, textiles, electronics, photovoltaics, cosmetics and biomedical applications such as cancer therapies, orthopedic surgery, and protein separation (Oi et al.,2016; Periyat et al., 2016). TiO_2 has three different stable/metastable phases; anatase, rutile, and brookite. Anatase is known as “octahedrite” and was renamed by R. J. Hauy in 1801 (Periyat et al., 2016). Its name comes from the Greek Word ‘’anastasis’’ which means extension due to its longer vertical axis. Rutile phase was discovered by Werner in 1803 and its name comes from the Latin Word ‘’Rutilus’’ which means red (Periyat et al., 2016). Another phase is brookite which was discovered by A. Levy in 1825 and the name of brookite comes from English mineralogist H. J. Brooke (Periyat et al., 2016). Anatase and

rutile are the most common polymorphs which are used in studies dealing with photocatalysis. These polymorphs have different physical properties, rutile is the most stable phase while anatase and brookite are metastable phases at ambient conditions. Anatase has four units, rutile has two units, brookite has eight units (Oi et al., 2016). Anatase is the primary phase of the crystalline TiO_2 phase, rutile phase is obtained by heat treatment and anatase is converted to rutile by reconstruction through bond breaking and reforming irreversibly. The light absorption ability of the rutile phase is better than the anatase phase due to differences between bandgap energies. Bandgap energies of rutile and anatase phases are 3.0 eV and 3.2 eV, respectively. Even though lower light absorption capacity, anatase phase is photocatalytically more active than rutile phase due to anatase phase's higher surface adsorption capacity of hydroxyl group, lower charge carrier recombination rate, the longer lifetime of photogenerated electrons and rutile phase's larger grain size, lower specific surface area and lower surface adsorption capacity (Zhang et al., 2014). Properties of TiO_2 phases are given in table 2.1.

Table 2.1. Properties of TiO_2 phases (anatase, rutile, and brookite) (Oi et al., 2016)

Property	**Anatase**	**Rutile**	**Brookite**
Crystal Bulk Structure	Tetragonal 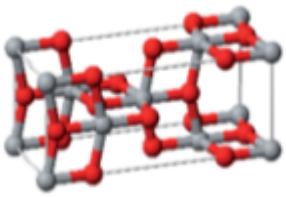	Tetragonal 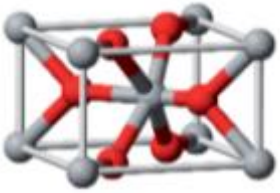	Orthorhombic 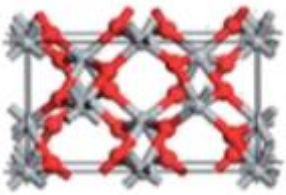
Atom per unit cell (Z)	4	2	8
Crystal Size (nm)	<11	>35	11-35
Lattice Parameter (nm)	a=b= 0.3785 c= 0.9514	a=b= 0.4594 c= 0.2959	a=c= 0.5436 b= 0.9166
Unit cell volume (nm^3)	0.1363	0.0624	NA
Density (gcm^{-3})	3.83	4.24	4.17
Band Gap (eV)	3.26	3.05	NA
Hardness (Mosh)	5.5-6	6-6.5	5.5-6

2.2.3.2. Zeolitic Imidazole Framework-8 (ZIF-8)

Metal-organic frameworks (MOF) are microporous materials that are created with metal ions and organic linkers. The type of MOF structure materials was first reported in 1960 by Tomic and rediscovered by Omar Yaghi and his research group (Carreon & Venna 2020). A schematic representation of 3D metal-organic framework structure formed with metal ions and organic linkers is given in Figure 2.7.

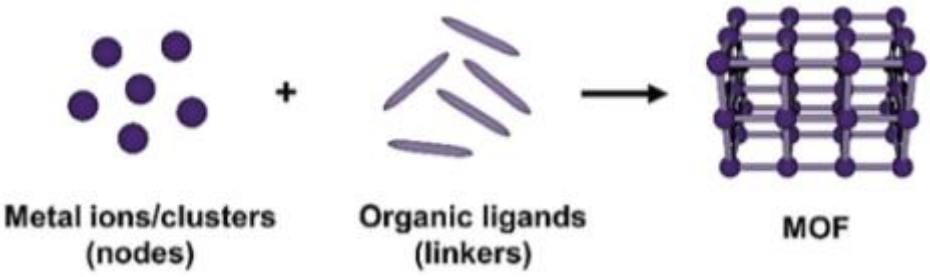

Figure 2.7. A schematic representation of 3D metal-organic framework structure formed with metal ions and organic linkers (Goetjen et al., 2020)

Due to microporosity and ease of design of desirable properties, MOFs are used in gas storage, gas separation, drug delivery, sensing, water purification, and catalysis (Feng et al., 2020; Goetjen et al., 2020; Sheng et al., 2017). Another important application area of MOFs is hydrogen storage. Due to harmful effects and limited sources of fossil fuels, hydrogen is preferred instead of fossil fuels in the automotive and transportation industry, hydrogen fuel provides a 500 km driving distance. Hydrogen fuel cells on vehicles are based on pressure tanks where hydrogen is pressurized between 300-700 bar (Ren et al., 2015). Storage for 6 kg of hydrogen needs a 215 L tank and 350 bar pressure, this volume can be reduced down to 150 L at 700 bar (Ren et al., 2015). Production of this type of tank has a high cost and this problem can be solved by the use of MOFs. MOFs enhance the storage of hydrogen due to their high volume, low cost, lightweight, cyclability, not requiring high pressures, reversible hydrogen uptake and appropriate hydrogen charge/discharge kinetics (Ren et al., 2015). A comparison of hydrogen storage techniques is given in Figure 2.8.

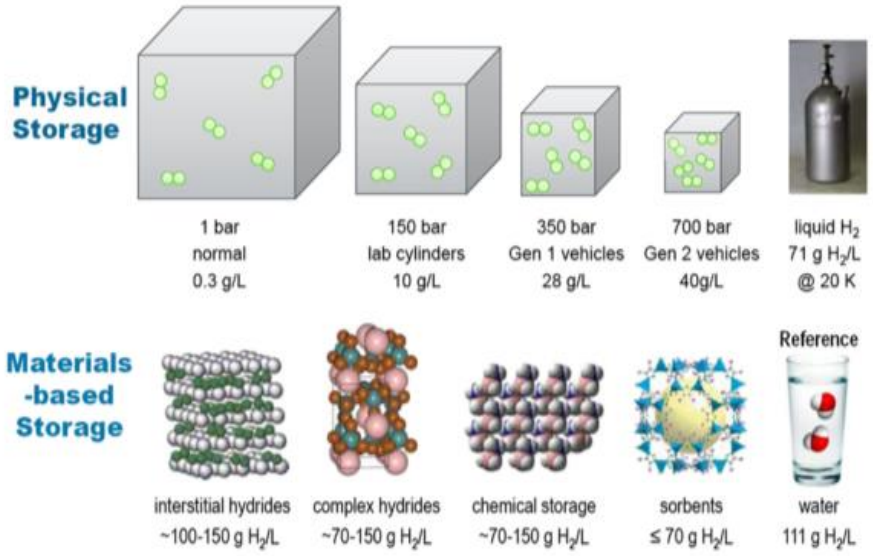

Figure 2.8. A comparison of hydrogen storage techniques (J. Ren et al., 2015)

Zeolitic-Imidazole Framework-8 (ZIF-8) is a type of MOF that is composed of zinc as the metal and 2-methylimidazole as the organic linker. Tetrahedral metal ions are linked by imidazole ligands in ZIF-8. The surface area, particle size and pore volume of ZIF-8 can be changed by using various methods such as solvothermal, microwave-assisted, sonochemical and mechano-chemical synthesis. Also, reaction time and the use of different solvents can alter the surface area and pore structure of ZIF-8 (Lai et al., 2014; Lee et al., 2015). ZIF-8 crystal structure is shown in Figure 2.9.

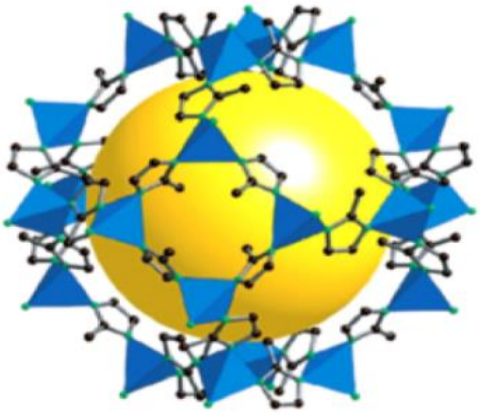

Figure 2.9. ZIF-8's crystal structure. Black and green dots represent carbon and nitrogen atoms, respectively. Blue tetrahedra represent zinc ions. The yellow sphere represents the free volume in ZIF-8 (Feng et al., 2020)

2.3. Summary of the Studies on TiO_2 and ZIF-8/TiO_2 Photocatalysts

Photocatalysis is a catalytic reaction that begins with the absorption of light by a catalyst, involving the conversion of a substrate to products and was first described by the French scientist Landau in 1913 (Houk, 1988; Landau, 1913). TiO_2, whose photocatalytic activity under light was discovered by Keidel in 1929, is a widely used material in photocatalysis today due to its UV light activity which can easily be increased by certain modifications (Kiedel, 1929). Fujishima and Honda conducted the first study involving TiO_2 and photocatalytic processes in 1972 (Fujishima & Honda, 1972). The improvement of photocatalytic properties of TiO_2 with various metal dopants (Ag, Cu, Fe) and oxides such as TiO_2, Ag_3PO_4 /CuO/Cu_2O/$CuFe_2O_4$/Fe_2O_3 was shown in various studies dealing with photocatalytic dye degradation (methylene blue and methyl orange degradation) in the last years (Ahmed et al., 2013; Ajmal et al., 2016Ajmal; Hassan et al., 2016; Koohestani et al., 2016; Tran et al., 2019; Yu, 2016). The importance and popularity of research on H_2 production are increasing day by day and there are various studies in the literature on H_2 production with TiO_2 photocatalysts doped with Cu_2O, CuO, Fe_2O_3 (Barecca et al., 2015Barreca; De Kraftt et al., 2012; Lalhita et al., 2010; Khemthong et al., 2013; Shibli et al., 2013; Teng et al., 2014; Zhu et al., 2014).

In a study, surface modification of TiO_2 was conducted by Arbatzis and colleagues in 2003 (Arabatzis et al., 2003). TiO_2 was synthesized by the doctor blade method on a glass slide and the surface of TiO_2 thin film was modified with gold (Au) particles and its photocatalytic performance was tested by methyl orange degradation. Gold particles were deposited onto the TiO_2 surface with electron beam evaporation. The thin film which has 0.8 μgcm^{-2} gold coverage showed the best photocatalytic performance and its photocatalytic efficiency was 100%. In this study Arbatzis and colleagues observed that these gold particles have the main role to reduce the electron-hole recombination and increase the photocatalytic efficiency (Arabatzis et al., 2003). In 2004, Wu et al. deposited Cu on TiO_2 with incipient-impregnation followed by low-temperature calcination/reduction and metallization processes, 1.2 wt% Cu was found as the optimum loading and it showed better activity in hydrogen production from aqueous methanol solution and Cu particles were shown to be oxidized and self-regulated for reaching to optimum valance and maximum activity during the reaction. Doping of Cu ions to TiO_2 lattice reduced the activity according to their results (Wu & Lee, 2004). Another dye degradation study was performed by Aarthi and Madras in 2007 (Aarthi & Madras, 2007).

Aarthi and Madras studied the effect of organic solvent and metal ions on the photodegradation of Rhodamine B. TiO_2 was prepared by solution combustion method. Photocatalytic activity of TiO_2 that is synthesized by solution combustion method showed better photocatalytic activity than Degussa P-25 in Rhodamine B and Rhodamine 6G degradation. These dyes were degraded faster with the synthesized TiO_2 compared to Degussa P-25. Also, it was observed that the existence of solvent and metal ions reduce the degradation rate (Aarthi & Madras, 2007). In 2009, Yoong et al. studied hydrogen production by TiO_2 from water (Yoong et al., 2009). Copper was doped into TiO_2 by using two different methods. One of them was complex precipitation and the other was the wet impregnation method. Dopant loading amount was varied between 2 and 15% and three different calcination temperatures were applied (300, 400, 500°C). Photocatalysts were prepared in powder form. Photocatalyst which was prepared with complex precipitation with 10% copper loading and calcined at 300°C showed better photocatalytic activity than the impregnation method and this material produced much hydrogen from water compared to TiO_2 (Yoong et al., 2009). Isimjan et al. (2010) investigated structural and photocatalytic properties of Pt/ZIF-8 loading to TiO_2 nanotubes (TiO_2 NTs) and the performance of this structure was investigated in the photodegradation of phenol. A TiO_2 disc was dipped into the ZIF-8 solution vertically, ZIF-8 started to crystallize after 30 minutes and the disc was removed from the solution after 15h. The disc was then washed with methanol for 30 minutes in an ultrasonic bath and dried at atmosphere ambient. ZIF-8 loaded TiO_2 NTs were dipped into H_2PtCl_6 for 1h and then dipped into 0.002M $NaBH_4$ for 30 min to prepare Pt/ZIF-8 loaded TiO_2 NTs. The resultant material was washed with water and dried by N_2. The efficiency of Pt/ZIF-8 loaded TiO_2 NTs was determined to be %18.1. The results of the study of Isimjan and colleagues showed that Pt/ZIF-8 loaded TiO_2 NTs have a high potential for water treatment (Isimjan, Kazemian, Rohani, & Ray, 2010). Another study on the hydrogen production was conducted by Cheng et al. in 2012 (Cheng et al., 2012). Cheng et al. synthesized TiO_2 (P25)-graphene nanocomposite by the solvothermal method in which ethanol was used as a solvent. Composite was prepared in sealed-autoclave at 180°C for 8h. The composite powder was recovered by filtration, rinsed with deionized water several times, and dried at 60°C for 12h. According to their results, the P25-graphene nanocomposite showed enhanced light absorption and lower electron and hole recombination rate, and the optimum mass ratio of graphene to P25 in the composite was found as 0.5 wt%. P25-graphene

nanocomposite exhibited higher photocatalytic activity than P25 in hydrogen evolution from aqueous methanol solution (Cheng et al., 2012).

ZIF-8 is from the MOF family and is used in photocatalytic applications due to its microporous structure (Mahmoodi et al., 2019). By placing Cu, ZnO, CdS, Fe_2O_3, CdZnS, carbon quantum dots, $Bi_4O_5Br_2$ nanoparticles on/in ZIF-8, the photocatalytic properties of ZIF-8 were improved towards dye degradation, heavy metal reduction, CO_2 and Cr (VI) reduction, NO removal, and nitrogen to ammonia conversion (Guo et al., 2018; Liu et al., 2019; Liu et al., 2019; Qiu et al., 2018; Chandra et al., 2019; Wang et al., 2019; Wei et al., 2019; Xu et al., 2019). The development of new nano-composite structures increased the light absorption properties. The results of these studies showed that composite structures created by using ZIF-8 and other nanoparticles had better photocatalytic properties compared to their constituents in their pure form (Guo et al., 2018; Liu et al., 2019; Liu et al., 2019; Qiu et al., 2018; Chandra et al., 2019; Wang et al., 2019; Wei et al., 2019; Xu et al., 2019). Recently, TiO_2 and ZIF-8 are widely used materials in hydrogen generation applications. In 2012, Li et al. immobilized nickel particles in ZIF-8 (Li et al., 2012). Nanoparticles were synthesized by deposition-reduction method (in powder form) for hydrolyzing ammonia borane to hydrogen. Highly dispersed Ni nanoparticles were successfully immobilized by ZIF-8 and this material showed high photocatalytic activity and durability in the hydrolysis of ammonia borane (Li et al., 2012). In another study conducted by Jing et al. in 2014, photocatalytic degradation of methylene blue (MB) with ZIF-8 was investigated (Jing et al., 2014). The photocatalytic experiment was conducted under a 500 W Hg lamp, 25 mg ZIF-8 was added in 50 mL aqueous MB solution in a 50mL flask. According to this study, the MB degradation with ZIF-8 follows pseudo-first order-kinetic and rate constant was found to be $1.7x10^{-2}$ min^{-1} under UV light. ZIF-8 worked effectively in a wide pH range and showed high adsorption and degradation properties in an alkaline environment. Since ZIF-8 was found to be stable in the MB solution, authors suggested that ZIF-8 could be used repeatedly (Jing et al., 2014). In 2016 Zeng et al. synthesized CdS@ZIF-8 core-shell nanoparticle for hydrogen generation from formic acid (Zeng et al., 2016). CdS nanoparticles and $Zn(NO_3)_2$ were mixed and allowed to react at room temperature for 2h without stirring. The final powder product was obtained by centrifugation followed by washing with ethanol twice and drying in a vacuum overnight at 100°C. Core-shell structure showed higher selectivity than CdS in hydrogen generation from formic acid (Zeng et al., 2016). Zhang et al. synthesized TiO_2@ZIF-8 hollow

nanospheres for the enhancement of photocatalytic hydrogen generation of TiO_2 (Zhang et al., 2019). TiO_2 was decorated with ZIF-8 by a sonochemical route. The hydrogen yield of this composite was found as 261.7 μmol g^{-1} h^{-1} under 380 nm artificial sunlight. Zhang et al. found that; H_2 evolution by TiO_2 can be improved with ZIF-8 as a charge separator and active site supplier and MOF-based semiconductor composite material have a high potential for solar-light driven photocatalysis (Zhang et al., 2019). Photocatalytic degradation performance of a nanoporous metal-organic framework (MOF-199) was investigated in 2019 by Mahmoodi and Abdi (Mahmoodi & Abdi, 2019). MOF-199 was synthesized by a modified solvothermal method. The photocatalytic performance of MOF-199 was tested in photodegradation of BB41 (Basic Blue 41) dye under UV illumination. By this study, Mahmoodi and Abdi observed that the decolorization rate decreased with increasing dye concentration, whereas increased with the increase in pH level (Mahmoodi et al., 2019). In 2016, Chandra et al. encapsulated TiO_2 particles in ZIF-8 with in situ incorporation and investigated dye degradation performance of composite TiO_2@ZIF-8 on methylene blue and Rhodamine-B. They observed that TiO_2@ZIF-8 composite exhibited high photocatalytic performance than TiO_2 nanoparticles, even when this composite was used in the fifth catalytic cycle (Chandra et al., 2016). Pipelzadeh et al. studied the photocatalytic reduction of CO_2 to CH_4 and CO with ZIF-8@TiO_2 core-shell nanocomposite. ZIF-8@TiO_2 nanocomposite was synthesized by step-by-step process. Heat treatment at 300 and 400^oC was applied and reactions were carried out in a newly designed pressure adjustable reactor. According to their study, high amounts of ZIF-8 on TiO_2 increased CO_2 adsorption and increased CO yield (Pipelzadeh et al., 2017). Huang et al. (2018) studied CO_2 reduction to CO and CH_4 with ZIF-8 decorated TiO_2. ZIF-8 was in situ loaded on TiO_2 foil. CO_2 adsorption and reduction of CO_2 to CO and CH_4 with ZIF-8 decorated TiO_2 was found to be more effective than pure TiO_2 (Huang et al., 2018). Cardoso et al. (2018) investigated the effects of ascorbic acid on photoelectrocatalytic reduction of CO_2 to alcohol with ZIF-8 decorated TiO_2 nanotube. Electron donor (ascorbic acid) in the electrolyte increased CO_2 to methanol and CO_2 to ethanol conversion of ZIF-8 decorated TiO_2 nanotube (Cardoso et al., 2018). Li et al. (2020) investigated the degradation of tetracycline with ZIF-8@TiO_2 composite. ZIF-8@TiO_2 composite was synthesized by hydrothermal method. According to their results, the absorption capacity of ZIF-8@TiO_2 composite was better than the TiO_2 sphere and ZIF-8@TiO_2 composite showed visible light absorption and better catalytic performance due to low recombination rate of charge carriers in ZIF-8 (Li et al., 2020). Zhong et al. (2020)

decorated TiO_2 microspheres with ZIF-8 by a liquid phase deposition. The photocatalytic performance of this composite was investigated by using methylene blue and Rhodamine-B dyes. Composite degraded 90% of both dyes in 40 minutes and this excellent photocatalytic performance was attributed to the increased surface area and reduced recombination of photogenerated charge carriers (Zhong et al., 2020). Zhan et al. (2020) synthesized ZIF-8/Ag/AgCl/TiO_2 modified PAN (polyacrylonitrile) nanofibrous mat by stepwise in situ process and its photocatalytic performance was investigated in the degradation of methylene blue dye under visible light and natural sunlight. The nanofibrous mat showed good photocatalytic activity under both lights. Photocatalytic efficiency of nanofibrous mat reached 98.02% under visible light in 120 min and its degradation efficiency was found as 90.16% after five cycles and 80% after ten cycles (Zhan et al., 2020). Jia et al. (2020) prepared a pyramid shape rutile TiO_2 doped with N and F and coated with ZIF-8. Electro anodization and deposition was used for the preparation of TiO_2 electrdode. According to their results, N and F doping reduced the recombination rate of electron/hole pairs and the presence of rutile and anatase phases promoted charge carrier transfer and degradation performance of ZIF-8/NF-TiO_2 which was 21.6 times of unmodified TiO_2 for sulfamethazine degradation (Jia et al., 2020). Fazaeli and Aliyan (2018) deposited ZIF-8 on anatase TiO_2 nanorod by solvothermal method and bromothymol blue degradation performance was investigated. TiO_2@ZIF-8 possessed higher surface area than TiO_2 rods and after four cycles the efficiency of TiO_2@ZIF-8 remained at 74% (Fazaeli & Aliyan, 2018). In 2020, Qi et al. synthesized TiO_2(B) and ZIF-8 composite. Photocatalytic performance of this composite was determined by tetracycline degradation. TiO_2(B)/ZIF-8 composite showed 8 times better performance than pure TiO_2(B) and 3.6 times better performance than pure ZIF-8 (Qi et al., 2020). Dashtestani et al. (2020) encapsulated TiO_2 in ZIF-8 by in-situ incorporation and efficiency of this composite was determined in paraquat (PQ) herbicide degradation. The effects of the amont of photocatalyst and pH were investigated in the study. According to their results, the removal efficiency of paraquat (PQ) increased with the amount of TiO_2@ZIF-8 photocatalyst and pH. They found the optimum pH level and photocatalyst amount as 7 and 0.05 gL^{-1}, respectively. At the optimum pH level and optimum photocatalyst amount, paraquat (PQ) removal efficiency reached to 99.8% in 15 minutes (Dashtestani et al., 2020). Table 2.2 summarizes the studies on ZIF-8/TiO2 composites in literature.

Table 2.2. ZIF-8/TiO_2 composites and their use in photocatalytic applications

Composite Material	Application	Form of Photocatalyst	Reference
ZIF-8/TiO_2(Commercial TiO_2)	Dye Degradation	Powder	(Chandra et al., 2016)
ZIF-8/TiO_2(Commercial TiO_2)	CO_2 reduction	Powder	(Pipelzadeh et al., 2017)
ZIF-8/TiO_2 (On Ti plate)	CO_2 reduction	Ti foil	(Huang et al., 2018)
ZIF-8/TiO_2 nanotubes	CO_2 reduction	Ti plate	(Cardoso et al., 2018)
ZIF-8/TiO_2 hollow spheres	Hydrogen production	Powder	(M. Zhang et al., 2019)
TiO_2/ZIF-8	Antibiotic degradation	Powder	(R. Li et al., 2020)
ZIF-8/TiO_2 micro-spheres	Dye degradation	Powder	(Zhong et al., 2020)
ZIF-8/Ag/AgCl/ TiO_2-PAN	Dye degradation	Nanofiborus mat	(Zhan et al., 2020)
ZIF-8/TiO_2 nanotubes	Antibiotic degradation	Ti foil	(Jia et al., 2020)
ZIF-8/TiO_2 nanorods	Dye degradation	Powder	(Fazaeli & Aliyan, 2018)
ZIF-8/TiO_2(B)	Antibiotic degradation	Powder	(Qi et al., 2020)
ZIF-8/TiO_2	Organic compound degradation	Powder	(Dashtestani et al.,2020)

3. Materials and Methods

3.1. Thin Film Preparation

3.1.1. Transparent Thin Film Preparation

TiO_2 thin films were prepared by using sol-gel and dip coating techniques. In the first step, pure and doped TiO_2 sols were prepared. Titanium tetra isopropoxide (TTIP, $Ti[OCH(CH_3)_2]_4$) was used as the titanium precursor. Cerium nitrate ($Ce(NO_3)_3 \cdot 6H_2O$), iron(III) nitrate ($Fe(NO_3)_3 \cdot 9H_2O$), copper nitrate ($Cu(NO_3)_2 \cdot 3H_2O$) and zinc nitrate ($Zn(NO_3)_2 \cdot 6H_2O$) were used as dopant metal precursors.

Preparation of TiO_2 sols

Pure TiO_2 sols were prepared by the dropwise addition of water/nitric acid/ethanol solution to TTIP/ethanol solution under vigorous stirring. Doped TiO_2 sols prepared by following the same route where the only difference was that water/nitric acid/ethanol solution contained the dopant ion in specified amounts. The recipe given in Table 3.1 was used as the base recipe for the preparation of pure TiO_2 sol.

Table 3.1. The recipe used in TiO_2 sol preparation

TTIP (mL)	**Ethanol (mL)**	**HNO_3 (mL)**	**H_2O (mL)**	**Ethanol (mL)**
5	50	0.065	0.555	50

Deposition of TiO_2 films on Glass Substrates

TiO_2 thin films were coated on 7.5x2.5 borosilicate glass substrates by using dip coating technique. It is of great importance that the glass surface coating is homogeneous and continuous. Therefore, the glass surfaces were first cleaned with detergent in an ultrasonic bath, then with water, acetone and ethanol in an ultrasonic bath, finally with ethanol and dried with nitrogen.

The dip coating process was carried out with the dip coating system (dip coater) at certain dipping and retraction speeds of 200 mm/min. After the coating process, TiO_2 coated glasses

were dried at room temperature for 1 day and then they were subjected to heat treatment at determined temperatures (temperature range of 400-600°C). Since borosilicate glass begins to soften at 600°C, higher temperatures were not applied.

ZIF-8 Growth on TiO_2 Coated Glass Substrates

Before growing ZIF-8 crystals on TiO_2 surfaces, methanolic solutions of zinc (Zn^{+2}) and 2-methyl imidazole (Hmim is the source of imidazole rings, which are organic binders in Metal-Organic Framework structures) were prepared separately. The recipe given in Table 3.2 was used for the aforementioned solutions.

Table 3.2. The recipe used for growing ZIF-8 crystals

	Zinc Nitrate ($Zn(NO_3)_2 \cdot 6H_2O$)	2-metihylimidazol (Hmim)
Amount	0.9645	2.108
Solvent	45 mL Metanol	45 mL Metanol

In the preparation of ZIF-8 films, the previously prepared TiO_2 coated glass substrates were positioned vertically in an empty 100 mL beaker, and then Zn^{+2} and the Hmim solutions were poured into the beaker containing the TiO_2 coated glass substrate at the same time and mixed at room temperature for a certain time. Final mole ratios of Zn^{+2}: Hmim: methanol formed from the separately prepared solutions was 1:8:700 which is typical for ZIF-8 synthesis. Preparation of TiO_2 sols, TiO_2 deposition on glass substrates, and ZIF-8 growth on TiO_2 surface are schematically shown in Figures 3.1a, 3.1b, and 3.1c, respectively. For comparison, a bare ZIF-8 film was was also synthesized on glass surfaces. The glass surfaces were first functionalized by silanization. Cleaned glass slides were dipped in 2% (v/v) methanolic solution of trimethoxymethylsilane (Aldrich, 98%) for 4 hours. The slides were then washed with methanol and ethanol before coating process. The same procedure and recipe used in ZIF-8 growth on TiO_2 films were used for the preration of bare ZIF-8 films.

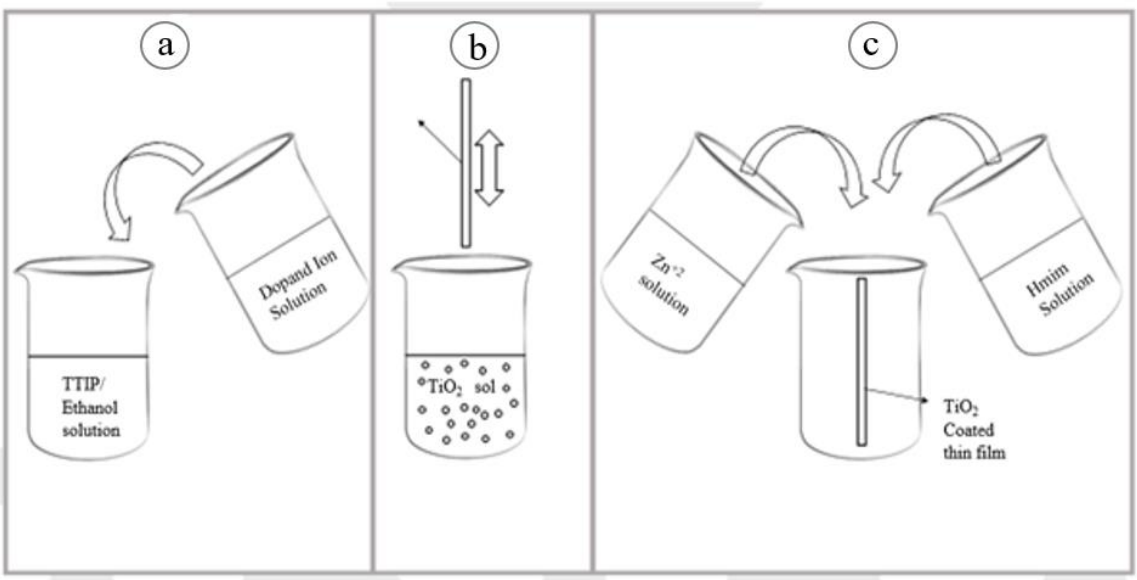

Figure 3.1. Schematic representation of a) TiO_2 sol preparation, b) TiO_2 deposition on glass substrates and c) ZIF-8 growth on TiO_2 surface

After TiO_2 thin film was coated with ZIF-8, methanol, and ethanol was passed over the films for 5 seconds to remove unreacted Zn^{+2} and the Hmim on the films. The films were dried at 80 ˚C for 24 hours. A schematic representation of the composite ZIF-8/TiO_2 film is shown in Figure 3.2.

Figure 3.2. Schematic representation of a multilayer composite thin film

Transparent TiO_2 thin films which were coated with ZIF-8 were coded with the prefix ZT, doped (cerium, iron, zinc, copper) TiO_2 thin films which were coated with ZIF-8 were coded with the prefixes ZTCe (for cerium doped TiO_2), ZTFe (for iron doped TiO_2), ZTZn (for zinc doped TiO_2) and ZTCu (for copper doped TiO_2).

3.1.2. Particulate ZIF-8/P25/TiO_2 Composite Thin Film Preparation

Particulate ZIF-8/P25/TiO_2 composite thin film was prepared by using Degussa P25 (a commercial powder), TTIP, zinc nitrate ($Zn(NO_3)_2 \cdot 6H_2O$) and 2-methyl imidazole. Cleaning processes of the glass substrate were the same as in the transparent thin-film cleaning process In the first step, 0.5 gram Degussa P25 was dispersed in 50 mL ethanol and ultrasonicated for 30 minutes while ZIF-8 was being prepared in the separate beaker with the following method. 0.9645 g zinc nitrate and 2.108 g Hmim were separately dissolved in 45 mL methanol. These two solutions were mixed and stirred in a separate breaker for 30 min.

In the second step, after the preparation of ZIF-8 and P25 Degussa, 20 mL P25 Degussa and 10 mL ZIF-8 suspension were added to a 30 mL ethanol. After a certain time, 4 mL of TTIP was added to suspension under vigorous stirring. Finally, the coating process was conducted. The followed steps are shown schematically in Figure 3.3. The coating was conducted by using the dip coater. In the dip coating process, 200 mm/min dipping and retraction speeds were used. ZIF-8/P25/TiO_2 composite thin films are called PZT30, where P stands for P25, Z stands for ZIF-8 and T stands for TTIP and 30 represents the optimum crystal growth time of ZIF-8 which was previously determined in transparent thin film preparation experiments. Two more particulate thin films were also prepared by using Ag doped ZIF-8 (5 mol%) (PZTAg) and ZIF-L (PZTL). In ZIF-L synthesis 0.662 g zinc nitrate and 1.642 g methyl imidazole were used.

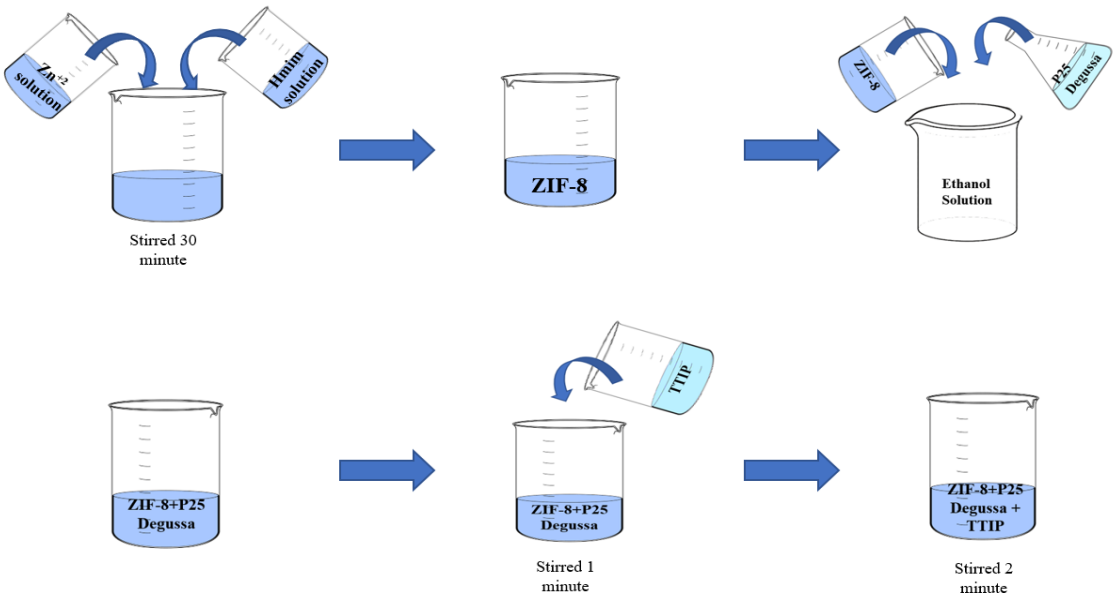

Figure 3.3. P25 Degussa + TiO_2 + ZIF-8 composite solution preparation

3.2. Characterization of The Films

Optical characterization of the prepared films conducted by Agilent, Cary60 UV-VIS Spectrophotometer. Light transmittance of the films were recorded in 300-800 nm wavelength. Band gaps of the films were calculated by using Tauc plots. The transformation was performed according to the relation given below:

$$\alpha h\nu = B(h\nu - E_g)^n \quad (3.1)$$

where hν is photon energy, β is a constant, E_g is the bandgap energy, n is the allowed direct band which is 0.5 and α is the absorption coefficient which was calculated by using the relation given below:

$$\alpha = \ln(1/T) / d \quad (3.2)$$

where T is transmittance and d is film thickness (Haarindraprasad et al., 2015)

Crystalline phase characterization was carried out by X-ray Diffraction (XRD) analysis performed with Rikagu Miniflex 600. XRD patterns were recorded in the 5-40^{o} 2theta region. Crystallite size was calculated by using Scherrer's equation given below:

$$D = \frac{K\lambda}{\beta cos\theta} \tag{3.3}$$

where, D is crystallite size, K is a constant, λ is the wavelength of x-ray source, β is full width at half maximum (FWHM) and θ is the peak position.

Surface morphology and film thickness were monitored by FEI Quantra 650 Scanning Electron Microscope Thicknesses and average grain sizes of thin films were calculated.

X-ray photoelectron spectroscopy (XPS) analyses were conducted by using XPSSPECS EA 300. The carbon C1s line at 284.8 eV was taken as a reference for the correction of the peak shifts. Peak fits were conducted by using the Gaussian-Lorentzian function via XPSPEAK41 software program.

3.3. Photocatalytic Dye Degradation Experiments

3.3.1 Photocatalytic Dye Degradation Experiments of Transparent Thin Films

The photoreactor system is shown in Figure 3.4 was constructed for photocatalytic dye degradation experiments. A Plexiglass box with 11 cm height and 10.5 cm width in which a glass container with 4,8 cm diameter and 2,4 cm height was placed at the bottom was used. A LED light with the maximum emission at 254 nm was placed at the top as seen in the Figure 3.4. The active surface area of the thin films was 2.5x2 cm^2. The films were placed at the bottom of the glass container horizontally (perpendicular to the LED lamp). 5 mL of 2 ppm methylene blue was used as the model dye solution. The experiments were conducted for 1 hour. After turning off the LED lamp, three samples were taken from the glass container and analyzed by using the UV-Vis spectrophotometer. Dye concentrations were calculated according to the equation below:

% dye concentration = $C/C_o * 100$ (3.4)

where, C is the absorbance of methylene blue solution samples taken at different times and Co is the absorbance of 2 ppm methylene blue solution. The absorbance value at the maximum light absorption wavelength, 664 nm, was used. The same setup was used for the evaluation of the activities of the films under 365 nm light. The only differences were the volume of MB solution which was 25 mL and the solutions were constantly stirred during the experiments.

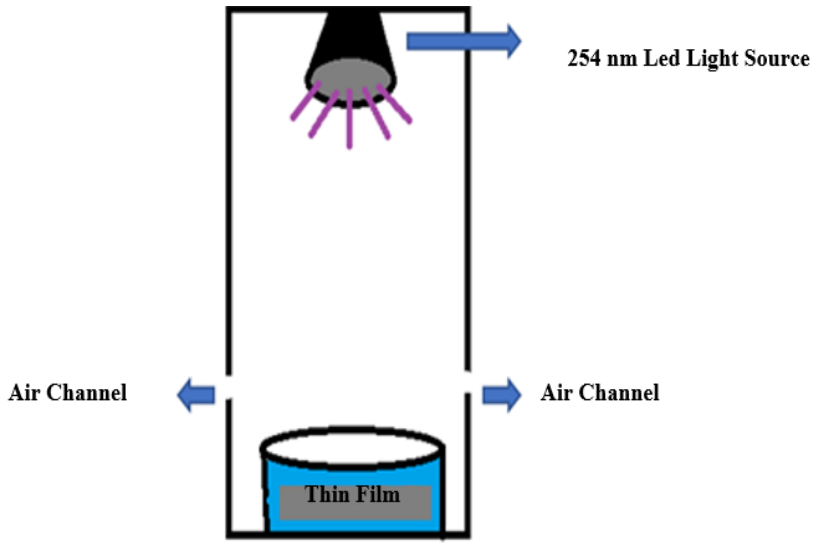

Figure 3.4. Photoreactor system constructed for photocatalytic dye degradation experiments of thin films

3.3.2. Photocatalytic Dye Degradation Experiments of Particulate Thin Films

The photoreactor system shown in Figure 3.5 was constructed for the photocatalytic dye degradation experiments of the particulate thin films. Led light and the cooler fan were placed on a magnetic stirrer and a 50 mL beaker that contains 2 ppm dye solution was placed in front of the light source. The dye solution was constantly stirred during the experiments. Dye concentrations were calculated according to the equation given in the previous part.

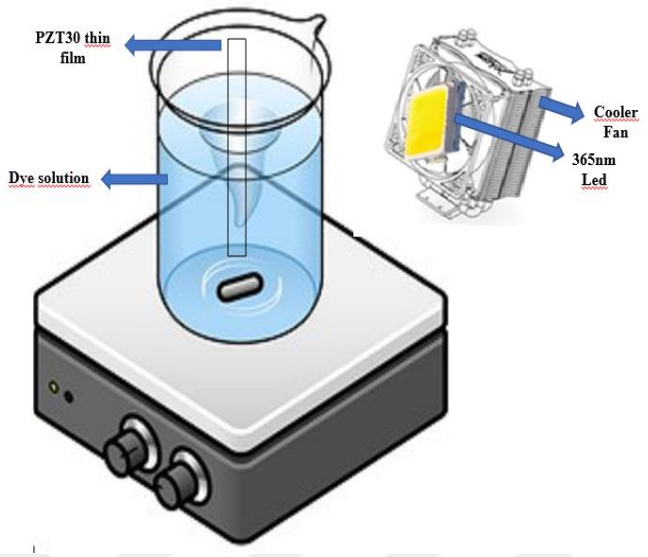

Figure 3.5. Photoreactor system constructed for photocatalytic dye degradation experiments of particulate thin films

4. RESULTS AND DISCUSSION

4.1. Characterization of the Films

4.1.1. Characterization of Transparent Thin Films

The surface morphology of the transparent thin films were investigated by SEM analysis. SEM images of the surfaces of the 1 % copper doped of transparent thin films are given in Figure 4.1. Copper-doped TiO_2 (TCu) coating was determined to be homogenous on the glass surface as shown in Figure 4.1a and the mean grain size of this film was determined to be 23 nm. Figure 4.1b shows the surface of ZIF-8 grown copper doped TiO_2 film (ZTCu). ZIF-8 particles grown on copper-doped titanium dioxide thin film were not homogeneously distributed on the surface and clusters were observed. ZIF-8 particles were almost spherical in shape and their mean grain size was 90 nm. No significant difference was found between the average thickness of TCu and ZTCu thin films, the mean thicknesses of TCu and ZTCu thin films were found to be in the 0.16-0.17 μm range (Figures 4.1c and 4.1d).

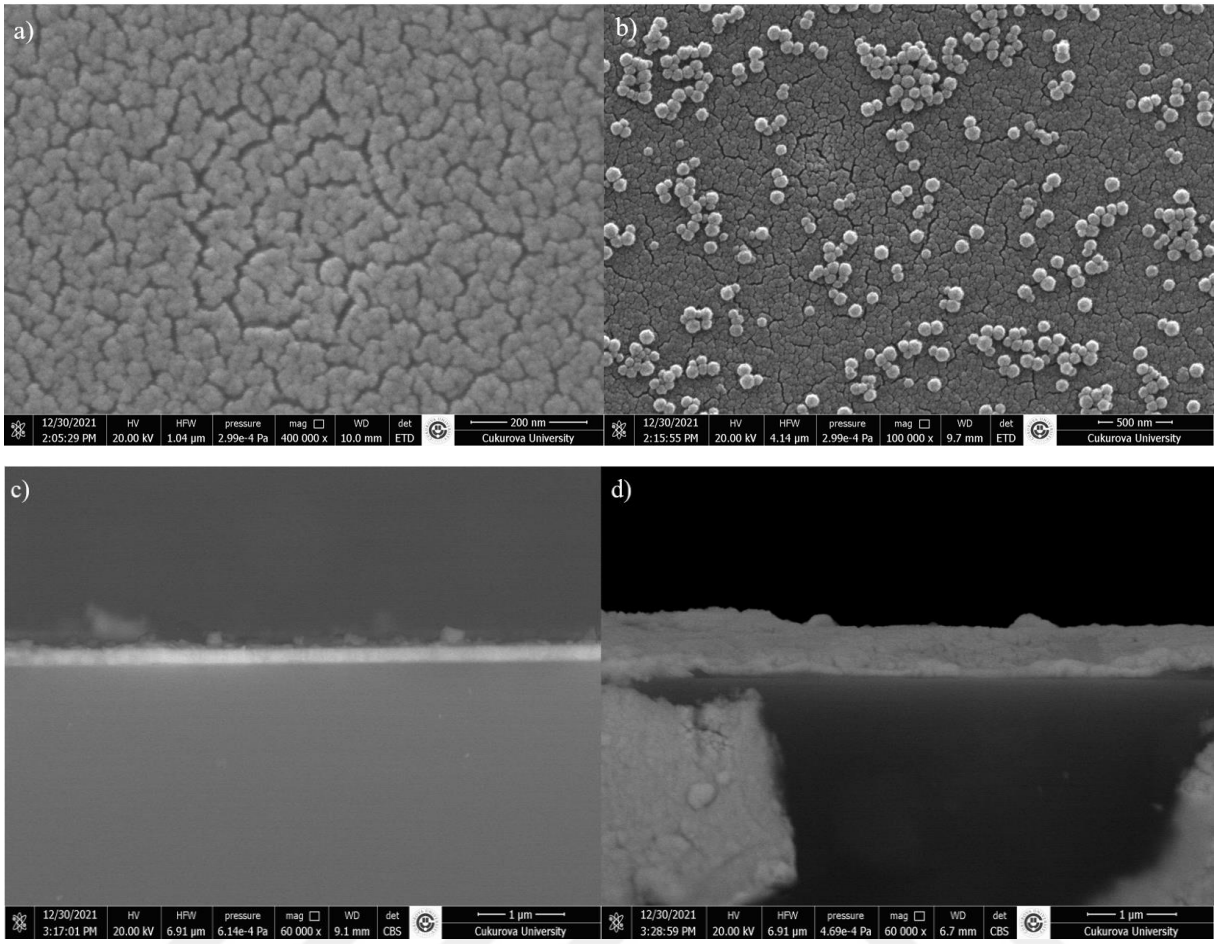

Figure 4.1. SEM images of a) surface of 1 % TCu, b) surface of 1 % ZTCu, c) crosssection of 1 % TCu d) crosssection of 1 % ZTCu thin films

SEM images of the 1 % iron doped TiO_2 transparent thin films are given in Figure 4.2. Iron doped TiO_2 (TFe) was homogeneously coated on the glass surface as shown in Figure 4.2a. The mean grain size of this film was determined to be 29 nm. Figure 4.2b shows the surface of ZIF-8 grown iron doped TiO_2 film (ZTFe). As it was previously observed for ZTCU, ZIF-8 particles grown on iron doped TiO_2 thin film were not also homogeneously distributed on the surface and the presence of clusters were also observed. ZIF-8 particles grown on iron doped TiO_2 were nearly spherical and their mean grain size was in the 90-100 nm range.

No significant difference was found between the average thicknesses of TFe and ZTFe thin films and the mean thicknesses of TFe and ZTFe thin films were found to be in the 0.15-0.16 µm range (Figure 4.2c and 4.2d).

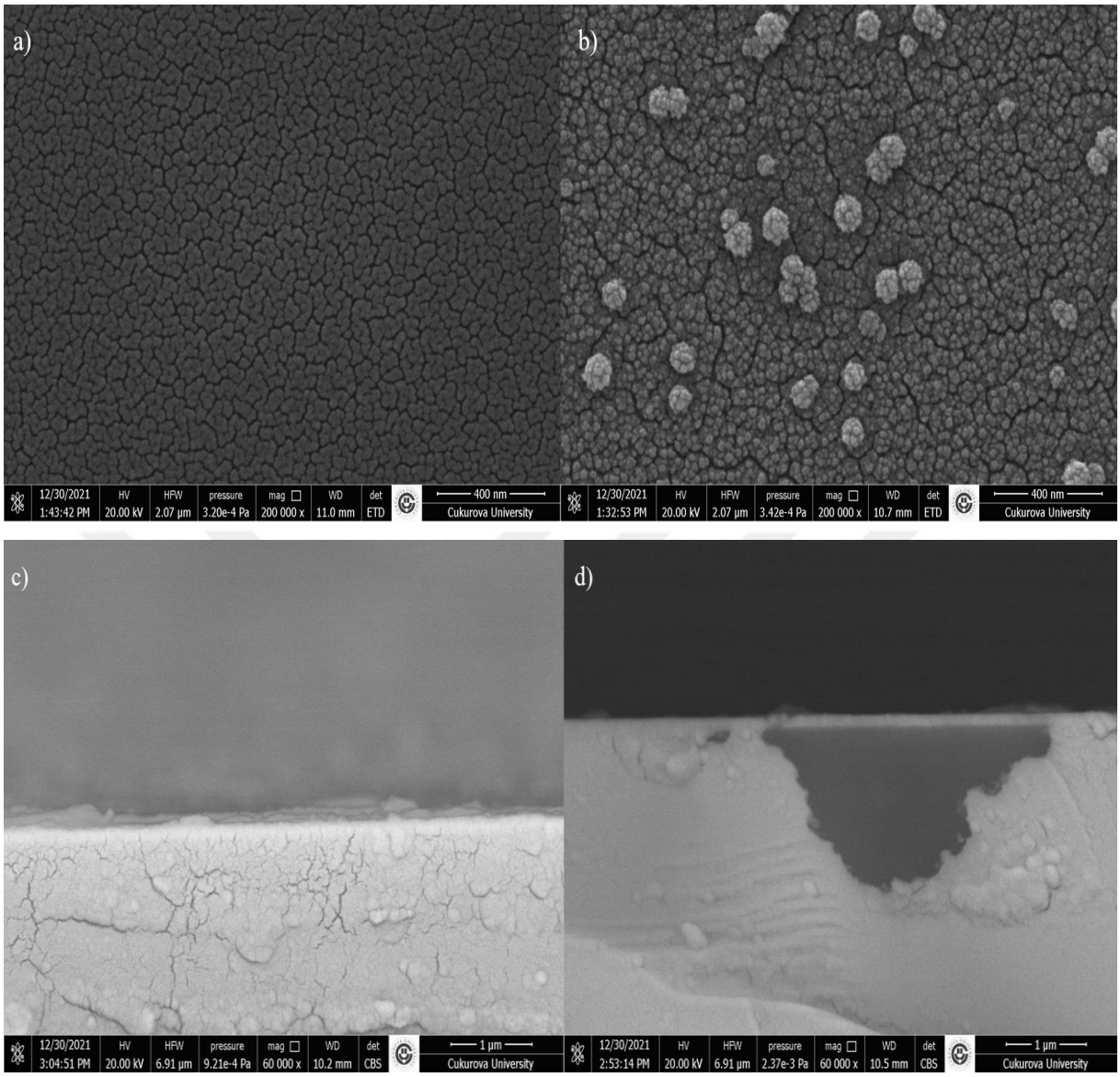

Figure 4.2. SEM images of a) surface of 1 % TFe, b) surface of 1 % ZTFe, c) crosssection of 1 % TFe, d) crossection of 1 % ZTFe

Light absorption properties of pure/doped TiO_2 films and ZIF-8/TiO_2 films were evaluated by recording their transmittance between 300-800 nm. Figure 4.3 shows the light transmittance of pure TiO_2 films heat treated at different temperatures. As can be seen from Figure 4.3, the curve shifted to lower wavelengths as the heat treatment temperature increases which means the film heat treated at 400^oC has higher light absorption capacity compared to other films.

According to Figure 4.4, the light absorption of TiO_2 was enhanced when its doped with Ce, Fe, Zn and Cu and it is seen that the curves shifted towards the visible region with doping. Also, light absorption increased with increasing doping levels. A comparison of light absorption of bare ZIF-8 and ZIF-8/TiO_2 composite films is given in Figure 4.5. As can be inferred from the Figure 4.5, light absorption of bare ZIF-8 was enhanced when pure/undoped TiO_2 layers were used as supports for ZIF-8 growth.

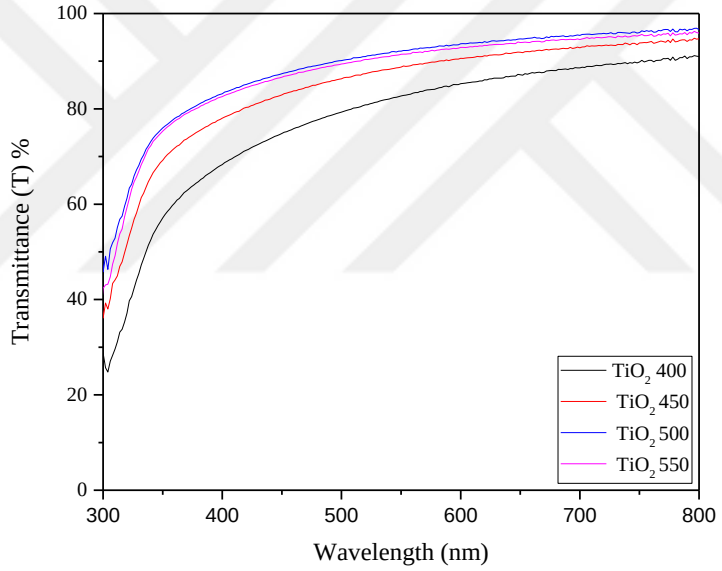

Figure 4.3. Transmittance spectra of pure TiO_2 films heat treated at different temperatures

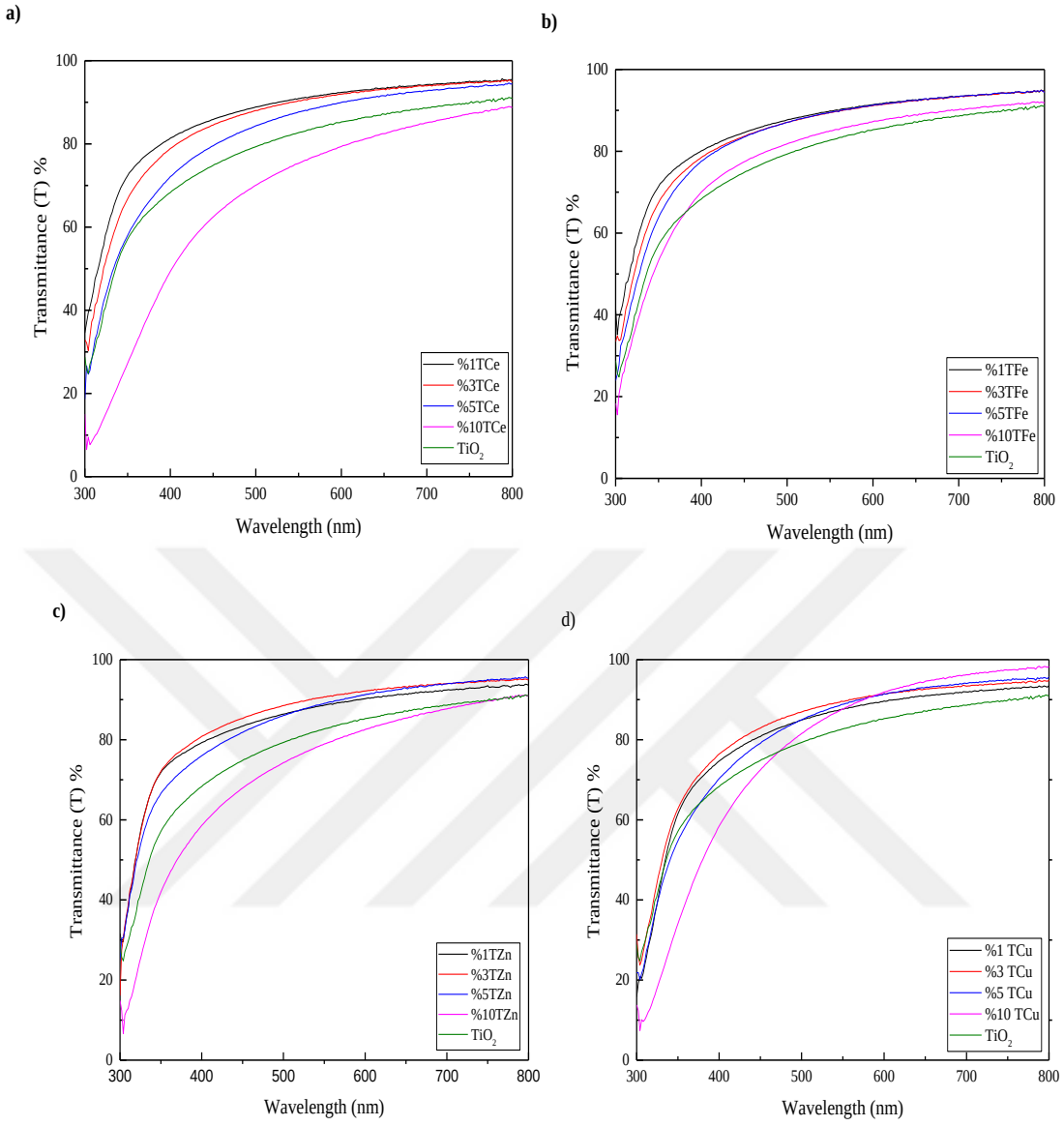

Figure 4.4. Transmittance spectra of pure/doped TiO_2 films: a) TCe, b) TFe, c) TZn, d) TCu

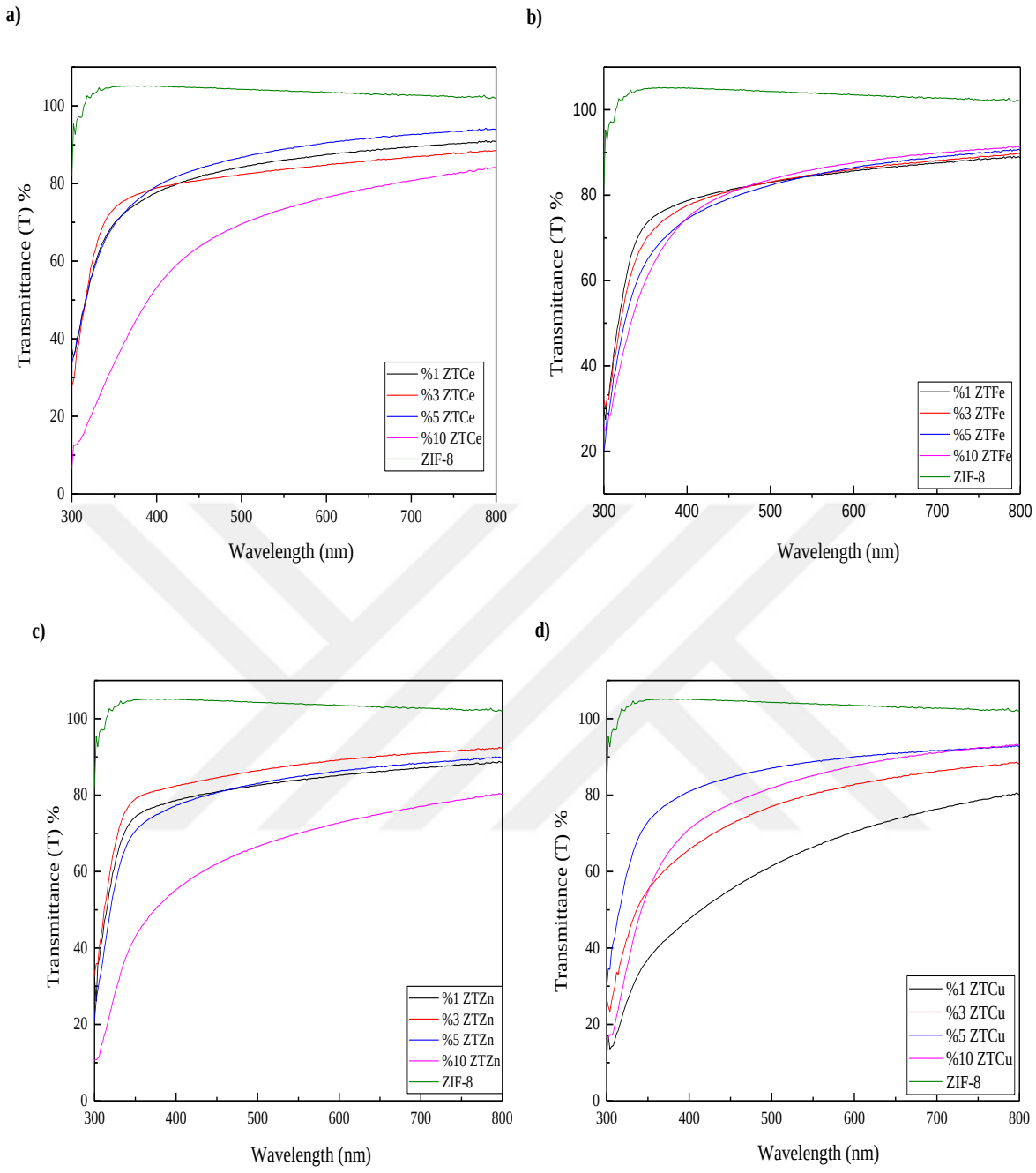

Figure 4.5. Transmittance spectra of ZIF-8/TiO_2 composite films: a) ZTCe, b) ZTFe, c) ZTZn, d) ZTCu

4.1.2. Characterization of Particulate Thin Films

XRD patterns of the particulate thin films heat treated at different temperatures are given in Figure 4.6. Thin film heat treated at 500˚C posseses a sharp peak at 25.3º 2theta which corresponds to the anatase (101) plane, whereas the films heat treated at 200, 300 and 400˚C showed no peaks originating from TiO_2. The main reason is that TiO_2 crystallites that would form due to the use of TTIP in the synthesis solution were very small (due to lower heat treatment temperatures) and were out of XRD detection limits. Also, the peaks of P25 and ZIF-8 were not detected in the XRD patterns of all the particulate films due to their low concentrations in the synthesis suspensions. The crystallite size of anatase TiO_2 in 500˚C heat treated particulate thin film was calculated as 26 nm.

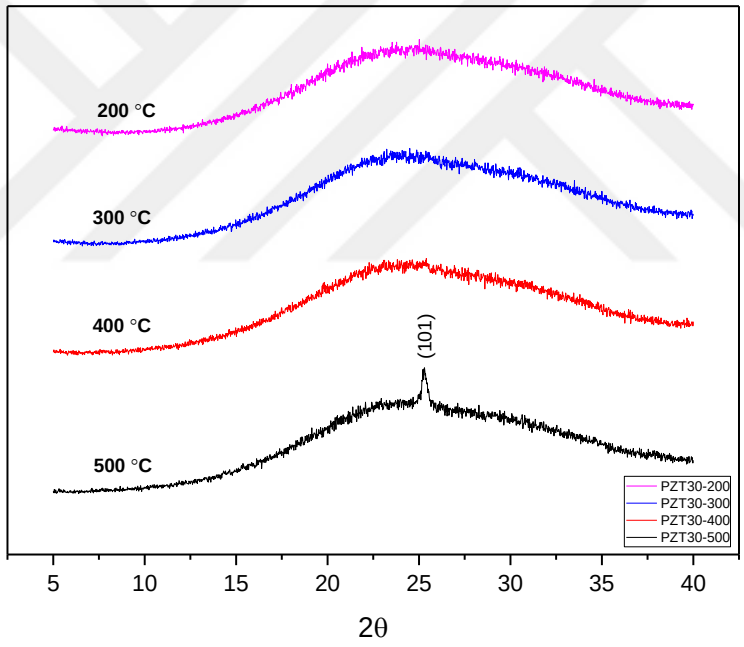

Figure 4.6. XRD patterns of particulate thin films heat treated at different temperatures

SEM images of the surfaces of particulate thin films heat treated at different temperatures are given in Figure 4.7 and the mean grain sizes calculated from these images are given in Table 4.1. As seen from the Figure 4.7, particulate thin films had sphere-like particles. The film heat treated at 400˚C had the smallest mean grain size. All the particulate thin films showed porous structure and pore size decreased with increasing heat treatment temperature.

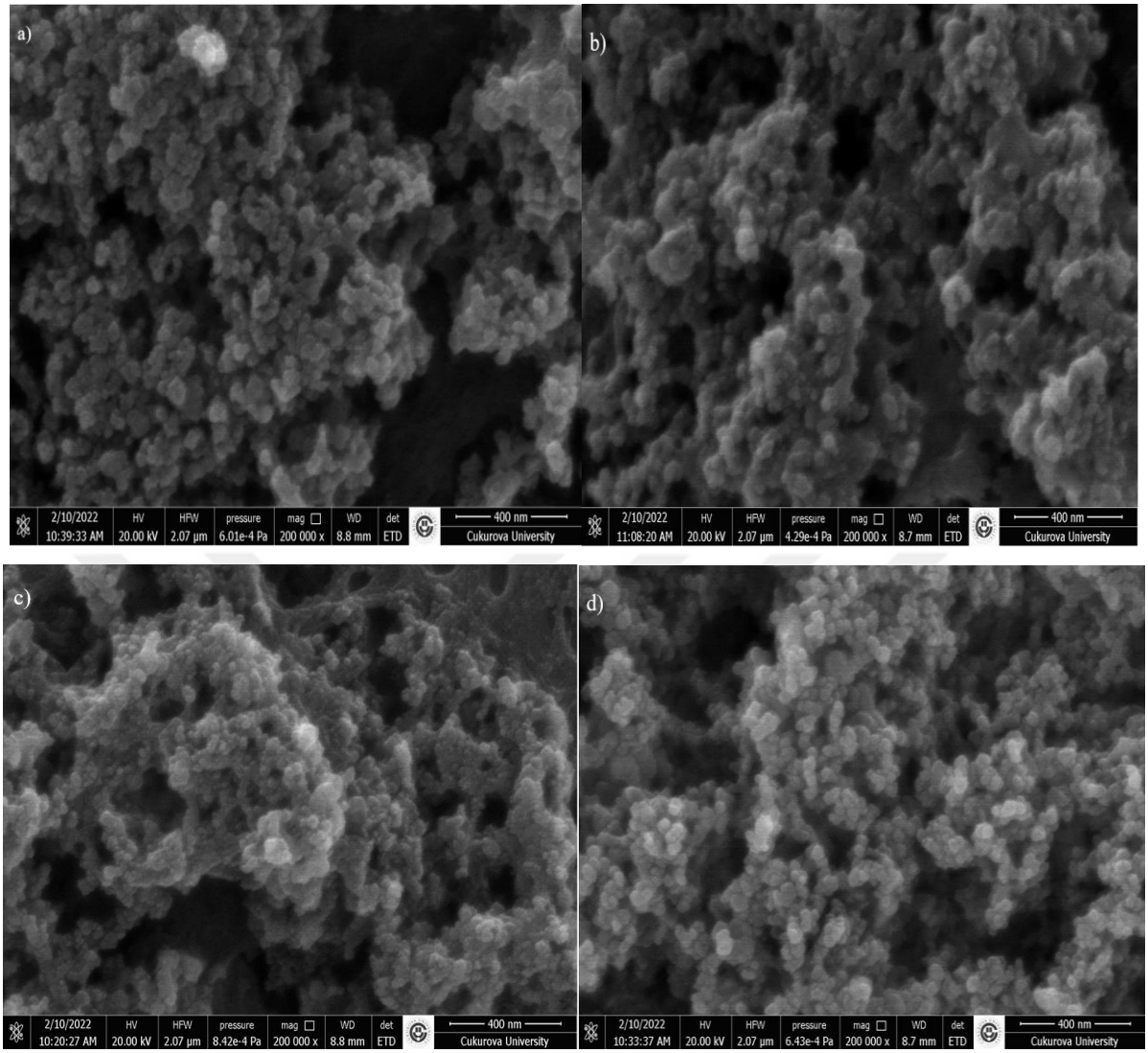

Figure 4.7. SEM images of particulate thin films heat treated at a) 200°C, b) 300°C, c) 400°C and d) 500°C

Table 4.1. The mean grain sizes of the particulate thin films heat treated at different temperatures

Heat treatment temperature (˚C)	Mean grain size of the thin films (nm)
200	54.8
300	49.1
400	30.9
500	44.7

Cross-sectional views of the particulate thin films heat treated at different temperatures are presented in SEM images given in Figure 4.8. There were no significant differences between the thicknesses of the films heat treated at 200˚C and 300˚C. The thickest film was obtained by heat treatment at 200˚C whereas the thinnest film was obtained by heat treatment at 500˚C. The average thicknesses of the particulate thin films are given in Table 4.2.

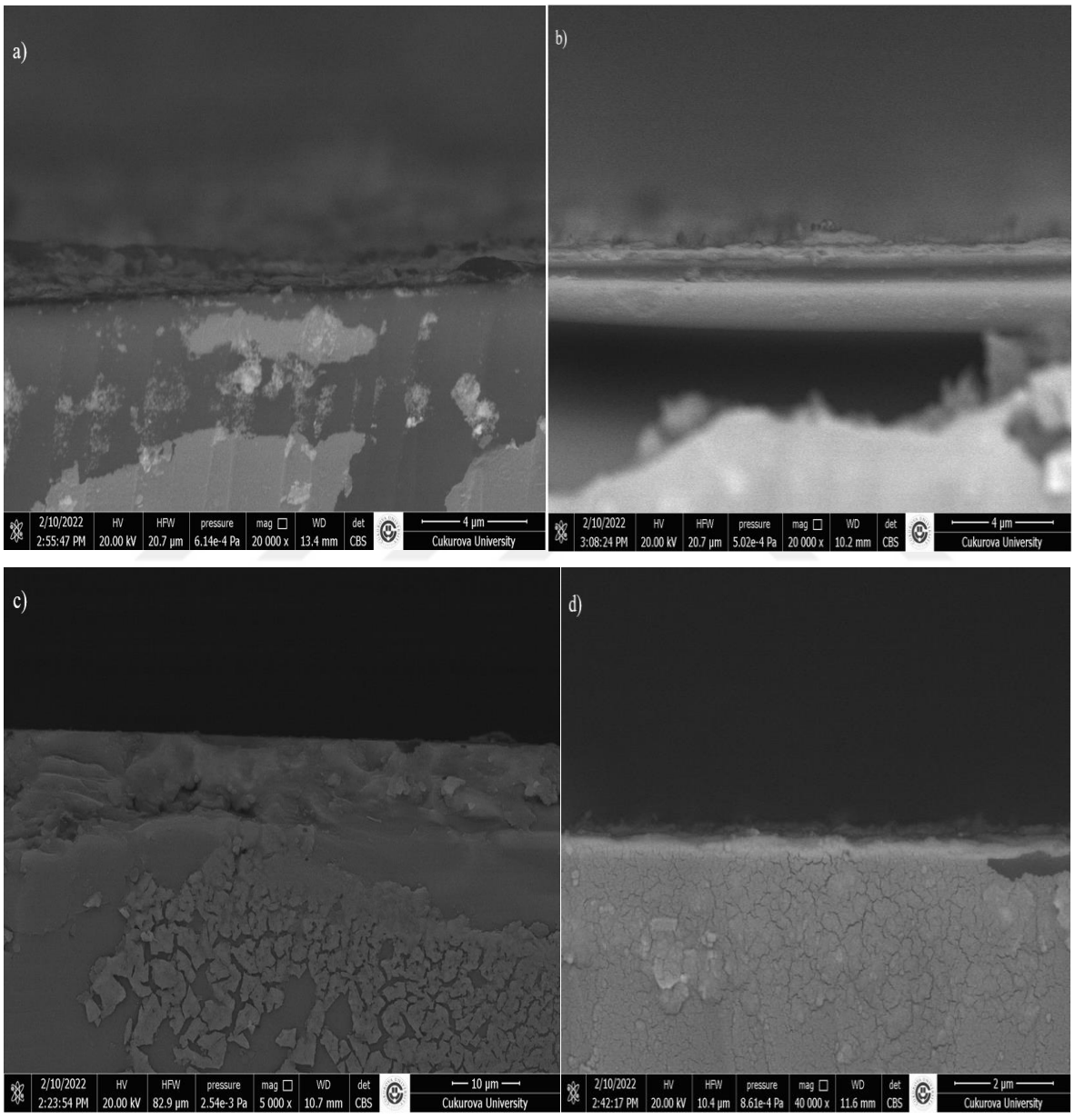

Figure 4.8. SEM images of the crosssections of particulate thin films heat treated at different temperatures a) 200^{o}C, b) 300^{o}C, c) 400^{o}C, d) 500^{o}C

Table 4.2. The mean thickness of PZT30 thin films heat treated different temperatures

Heat treatment temperature (°C)	Mean thickness of thin films (µm)
200	1.298
300	1.026
400	9.096
500	0.233

XPS spectra of PZT30 composite films diredat 80°C and heat treated at 500°C in C1s, Ti2p, O1s, Zn2p and N1s are given in Figures 4.9, 4.10 and 4.11, respectively. C1s spectra were fitted with three peaks at 284.8 (corrected value and set as a reference peak), 285 and 288 eV which can be assigned to C-C, C-N, and C-OH bonds, respectively. C-C and C-N bonds may originate from the adventitious carbon and imidazole rings (Luanwuthi et al., 2015), where the peak at higher binding energy may be the signal from adsorbed hydroxyls. Similar peaks (at 458.2 eV and 464 eV) were determined in the Ti2p spectra of the films. The separation between Ti2p3/2 and Ti2p1/2 is 5.8 eV which is consistent with the standard binding energies of TiO_2 (Sanjinés et al., 1994). O1s spectra were fitted with 530, 532 and 535 eV (not present in the film dried at 80°C). The first two peaks can be assigned to oxygen from TiO_2 lattice and Zn-OH, respectively. The third peak in the sample heat treated at 500°C can be assigned to H_2O (Munoz-Gil & Figueiredo, 2019). Zn2p spectra of both films (dried at 80°C and heat treated at 500 °C) were similar and contained two peaks at ~1022 and ~1045 eV. These peaks can be attributed to Zn2p3 and Zn2p1, respectively. N1s spectrum of the film driedat 80°C was fitted with two peaks at 399 and 400 eV, corresponding to -NH- and pyridinic (N bonded to two carbon atoms) nitrogen, respectively. N1s spectrum of the film heat treated at 500°C was fitted with two peaks at 399 and 407 eV which can be assigned to -NH- and oxidized nitrogen, respectively. Pyridinic nitrogen was converted to oxidized nitrogen due to heat treatment at 500°C and captured in the nanostructure (Miensah et al., 2021). The determined peak positions are given in Table 4.3.

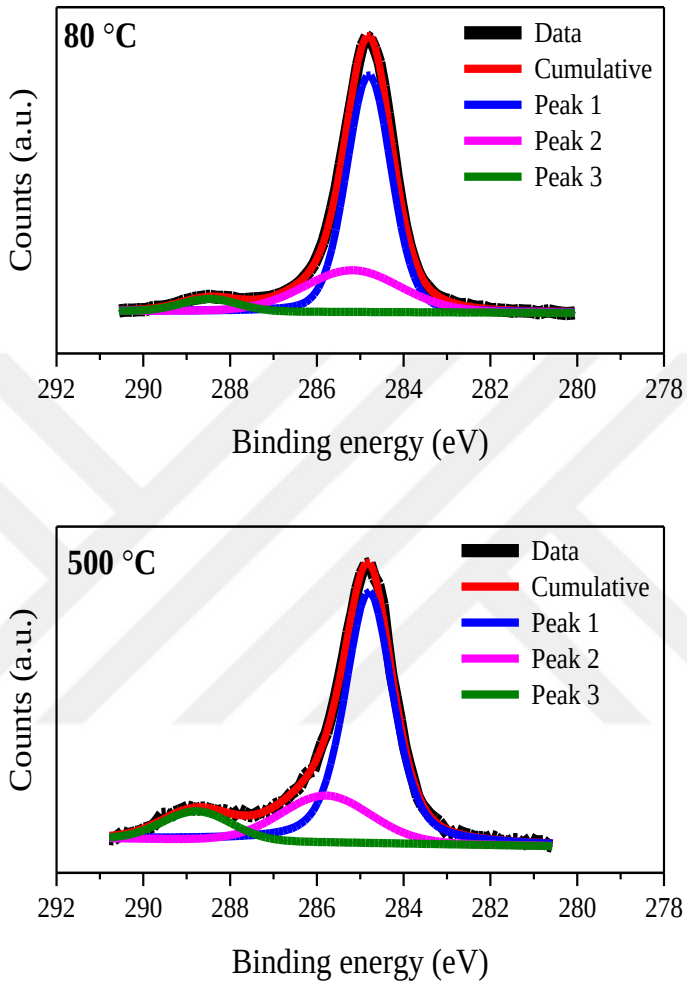

Figure 4.9. C1s XPS spectra of particulate thin films dried at 80°C and heat treated at 500°C

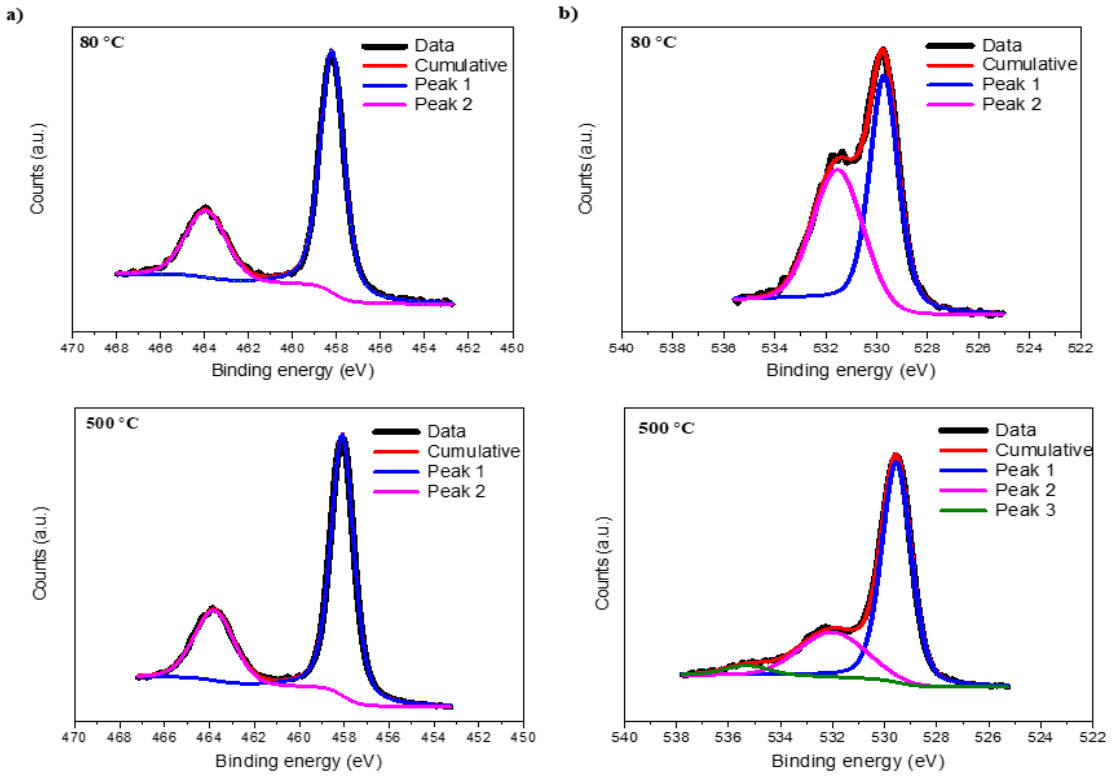

Figure 4.10. a) Ti2p and b) O1s XPS spectra of particulate thin films

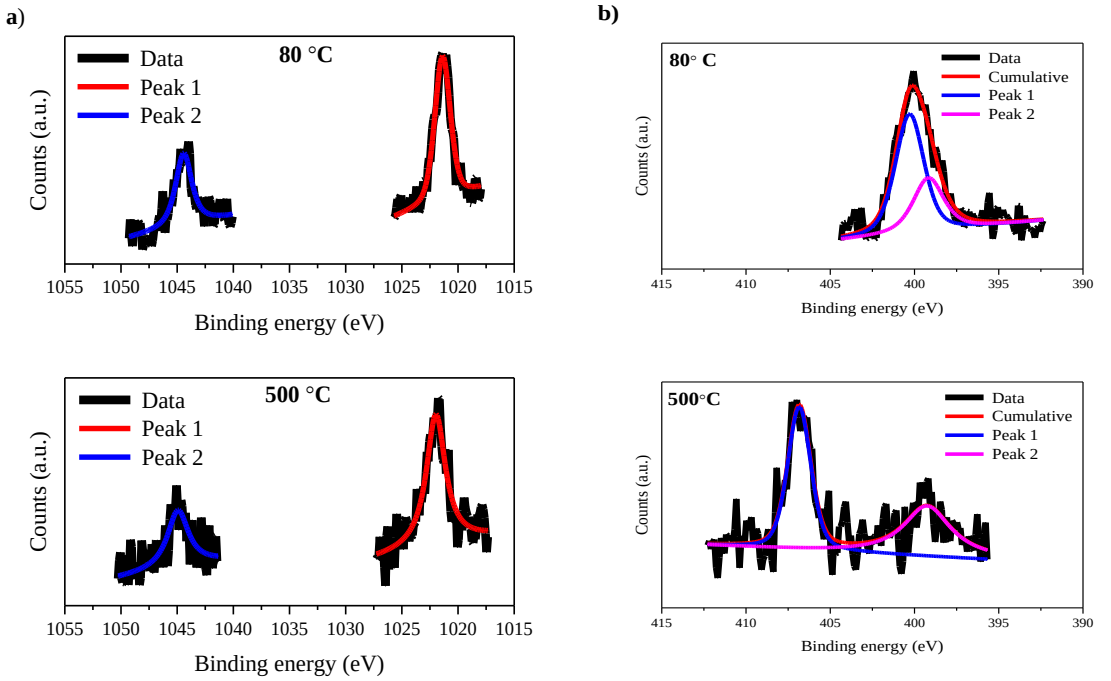

Figure 4.11. a) Zn2p and b) N1s XPS spectra of particulate thin films

Table 4.3. The determined peak positions of the corresponding films

Thin film	C1s (eV)	Ti2p (eV)	O1s (eV)	Zn2p (eV)	N1s (eV)
80ºC	284.8 285.181 288.473	458.217 463.933	529.715 531.526	1044.931 1021.97	400.29 399.175
500ºC	284.8 285.788 288.769	458.17 463.878	529.632 532.072 535.367	1044.499 1021.457	406.917 399.33

UV-Vis transmittance curves and the tauc plots for the calculation of band gap energies of particulate thin films are given in Figures 4.12 and 4.13, respectively. As it can be seen in the Figure 4.12, transmittance curves shifted to the visible light region with increasing heat treatment temperature. The calculated band gap energies also decreased with increasing heat treatment temperature. The lowest band gap was obtained with the film heat-treated at 500˚C, which is 2.14 eV. The results showed that the film heat treated at 500˚C can absorb light more efficiently than the other films.

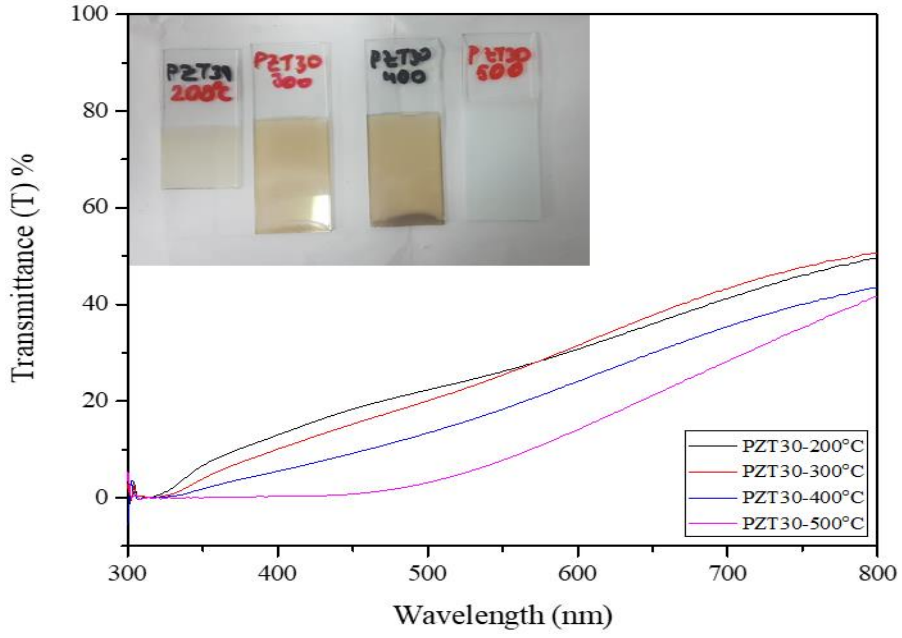

Figure 4.12. Transmittance spectra of particulate thin films heat treated at different temperatures

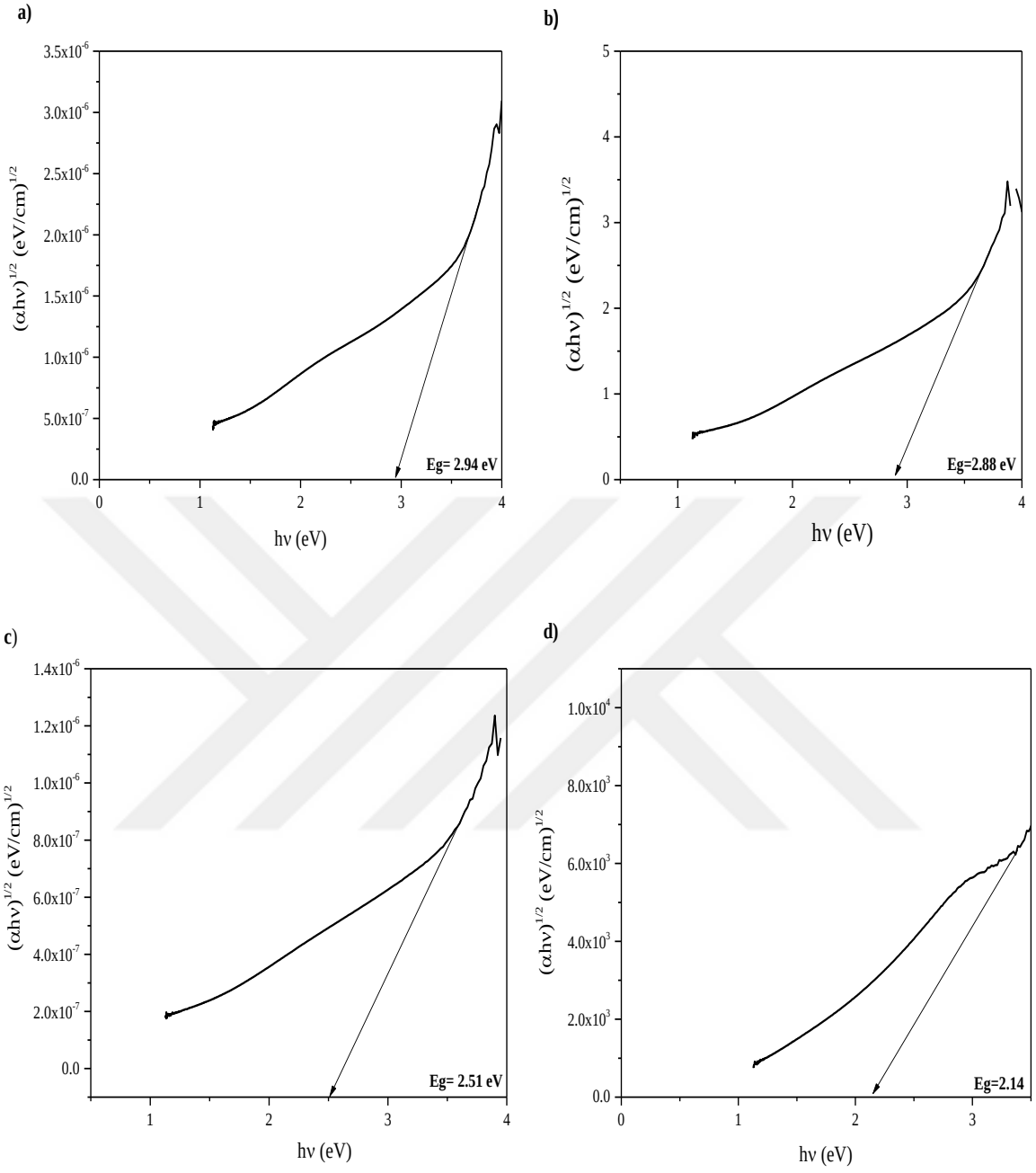

Figure 4.13. Tauc plots of particulate thin films heat treated at different temperatures

4.2. Photocatalytic Performance Results

4.2.1. Photocatalytic Performances of Transparent Thin Films

Before beginning the photocatalytic performance determination experiments, a direct photolysis experiment was first conducted to determine the contribution from self-degradation of methylene blue under 254 nm light. The experiment was conducted without any catalyst. As seen in Figure 4.14, 5 % of methylene blue was degraded under 254 nm light in 1 hour. This value will be a limit to the determination of adsorption efficiency or to the photocatalytic degradation efficiency.

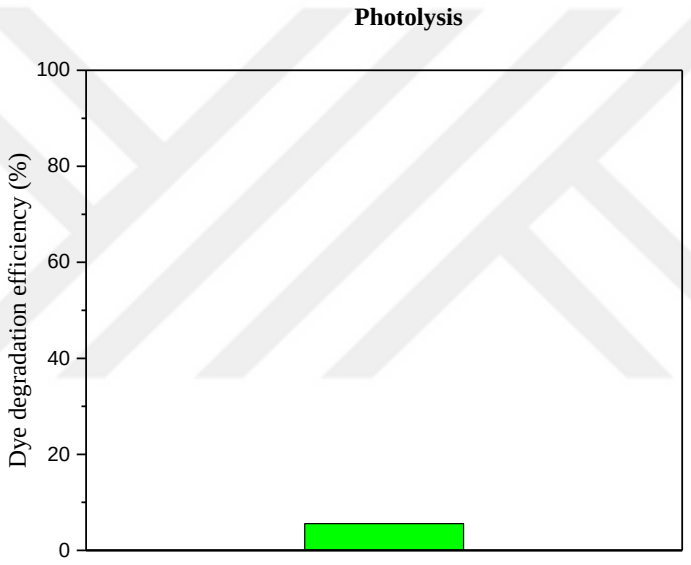

Figure 4.14. Direct photolysis of methylene blue under 254 nm light in 1 hour

Methylene blue adsorption studies were carried out with TiO_2 films heat treated at different temperatures to find out the time required for methylene blue to reach the adsorption-desorption equilibrium. As seen in Figure 4.15, adsorption was completed within 15 minutes for each film. Therefore, in photocatalytic dye degradation studies, holding for 15 minutes in the dark before turning on the light will be sufficient to ensure the adsorption-desorption equilibrium. The highest adsorption performance was obtained with TiO_2 film heat treated at 400^{o}C.

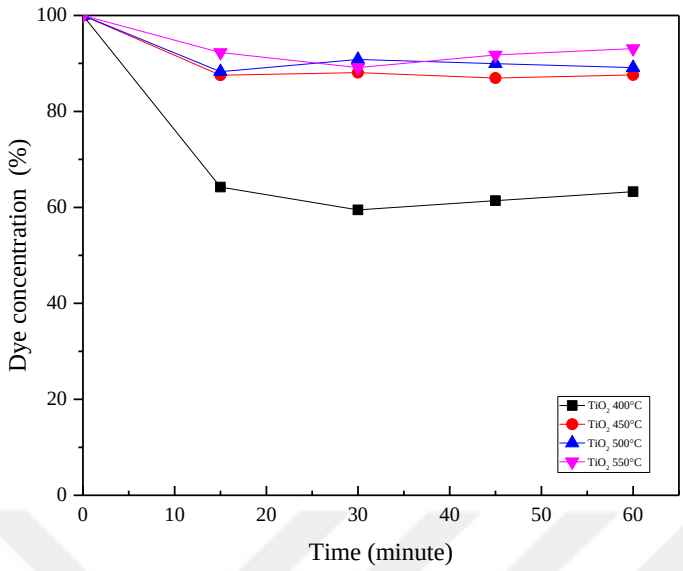

Figure 4.15. Time dependent adsorption curves of TiO_2 films heat treated at different temperatures

The photocatalytic performance and the dye degradation efficiencies (%) of TiO_2 films with different heat treatment temperatures are given in Figure 4.16. According to the dye degradation efficiencies, the highest activity was obtained with the film heat treated at 400^oC. With this film, approximately 56 % of methylene blue was removed from the solution. The methylene blue adsorption value of this film was around 40%. There were also differences between photocatalytic degradation and adsorption values for films which were heat treated at other temperatures. These differences showed that photocatalytic degradation can be performed with the prepared films. The film heat treated at 400^oC showed the best photocatalytic performance compared to the films which were heat treated at 450, 500 and 550^oC under 254 nm light.

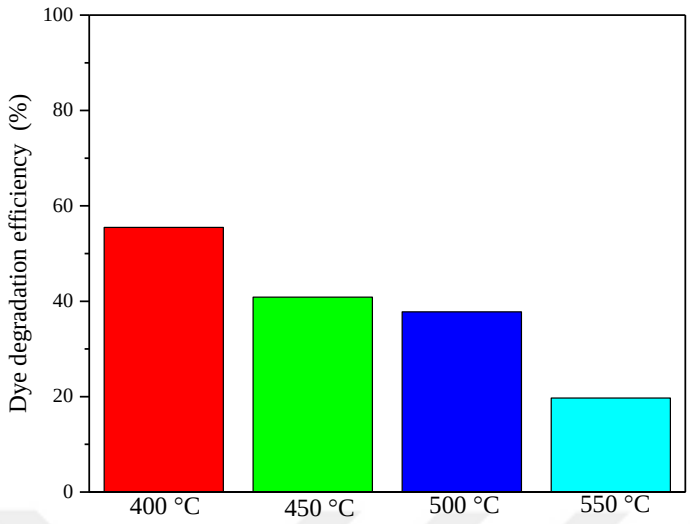

Figure 4.16. Dye degradation efficiencies of TiO_2 films heat treated at different temperatures at the end of 1 hour

In order to determine the effect of a crystalline and amorphous TiO_2 surface on the photocatalytic performance of the ZIF-8 layer, the photocatalytic activities of ZIF-8/TiO_2 composite films were evaluated by growing ZIF-8 crystallites on amorphous TiO_2 film (without heat treatment) and crystalline TiO_2 film heat treated at 400°C. Dye degradation efficiencies at the end of 1 hour are given in Figure 4.17. ZIF-8/TiO_2 composite film synthesized by using amorphous TiO_2 film showed very low photocatalytic performance compared to ZIF-8/TiO_2 composite film synthesized by using crystalline TiO_2 which was heat treated at 400°C. Thus, TiO_2 film heat treated at 400°C was chosen as the basis for preparing ZIF-8/TiO_2 composite films.

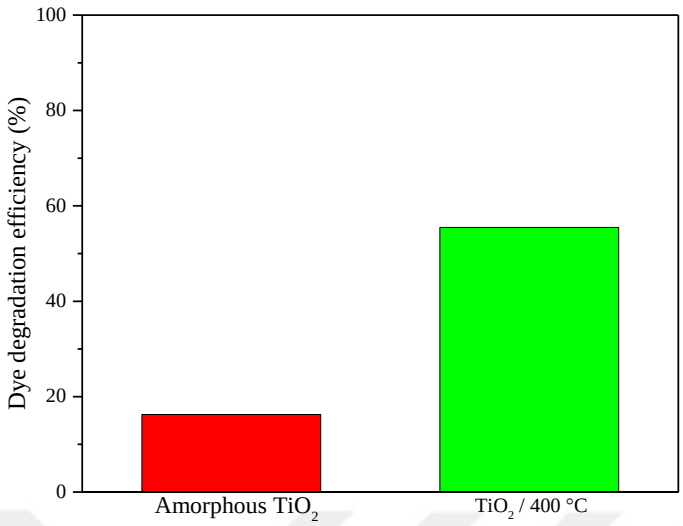

Figure 4.17. Dye degradation efficiencies of ZIF-8/TiO_2 composite films synthesized by using a) amorphous TiO_2 film and b) crystalline TiO_2 film

After determining the optimum heat treatment temperature, the effects of the number of TiO_2 layers on the photocatalytic activity were investigated. Thin films containing 2-4 layers were prepared and their photocatalytic performances were determined. According to Figure 4.18 the photocatalytic performances were slightly different and the activity was not dependent on the number of TiO_2 layers. Dye degradation efficiencies of multilayered TiO_2 thin films varied between 55 and 60 %. One layer TiO_2 thin film was chosen as the basis for preparing ZIF-8/TiO_2 films due to its higher transparency and ease of preparation compared to other films.

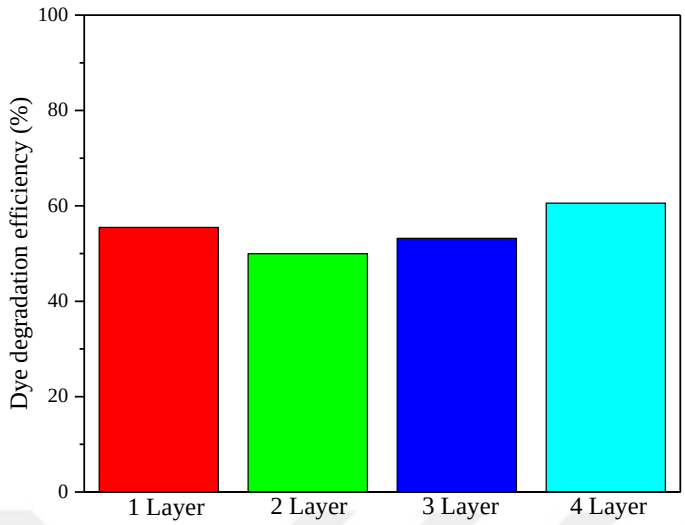

Figure 4.18. Dye degradation efficiencies of TiO_2 films with different number of layers at the end of 1 hour

The photocatalytic performances of different metals doped TiO_2 films were evaluated to find appropriate support for ZIF-8 growth. As it is inferred from Figure 4.19, the highest activities were observed with 1 % Ce and Fe doped TiO_2 films and the activities decreased as the dopant level increased. It was observed that Zn did not have a significant effect on the activity, whereas Cu doping decreased the activity of TiO_2.

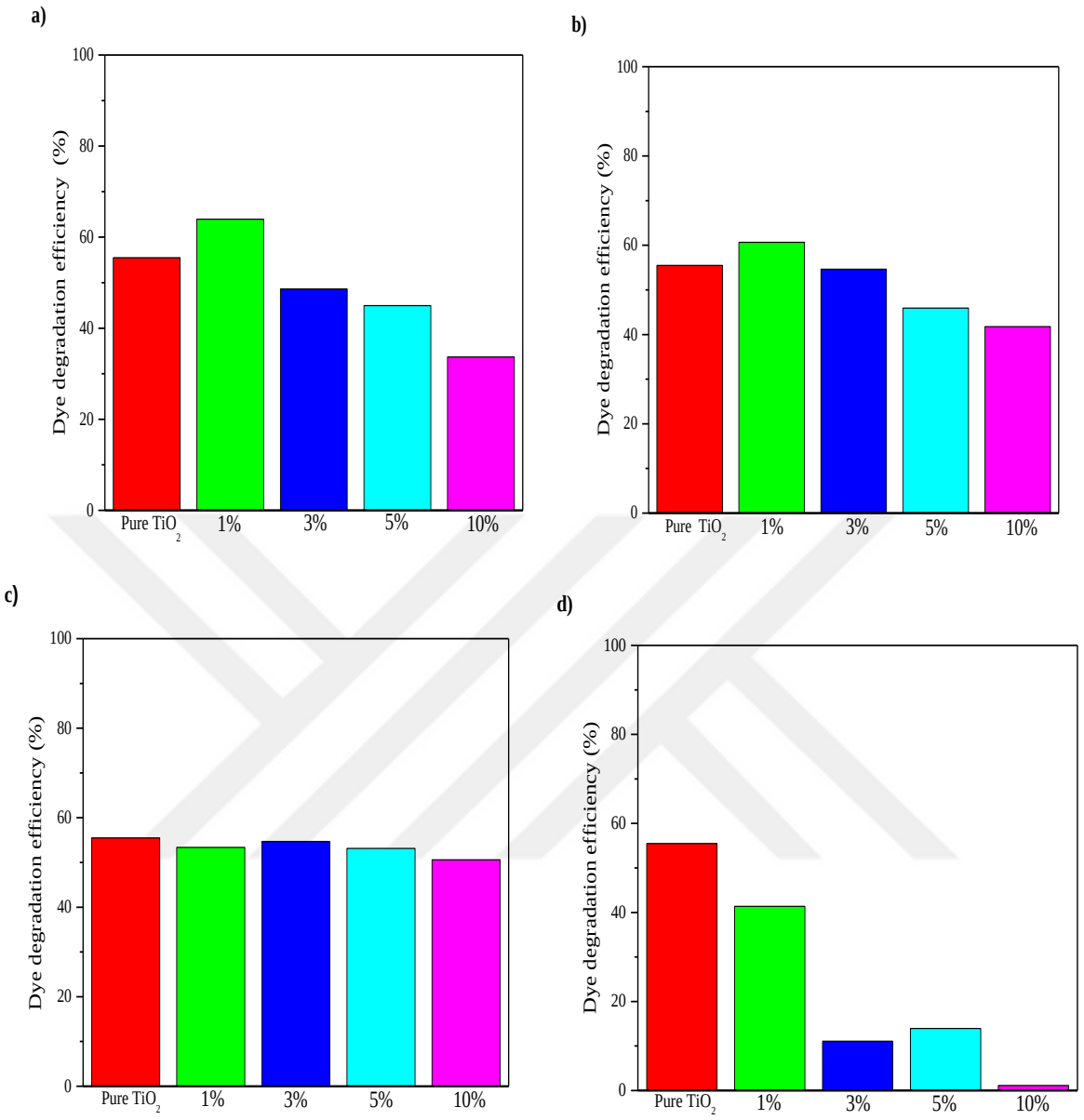

Figure 4.19. Dye degradation efficiencies of a) Ce, b) Fe, c) Zn and d) Cu doped TiO_2 films

The effects of ZIF-8 growth time on the photocatalytic performance were determined by investigating the photocatalytic performances of ZIF-8/TiO_2 composite films on which ZIF-8 was grown at different times (15, 30, 45 and 60 minutes). It was observed that the films prepared by using the reaction time of 45 and 60 minutes had heterogeneous surfaces and it was thought that 15 minutes may not be enough for ZIF-8 crystal growth and the efficiency of that film was not significantly higher than that of 30 minutes-grown film. Therefore, 30 minutes was chosen for ZIF-8 growth time in the following experiments.

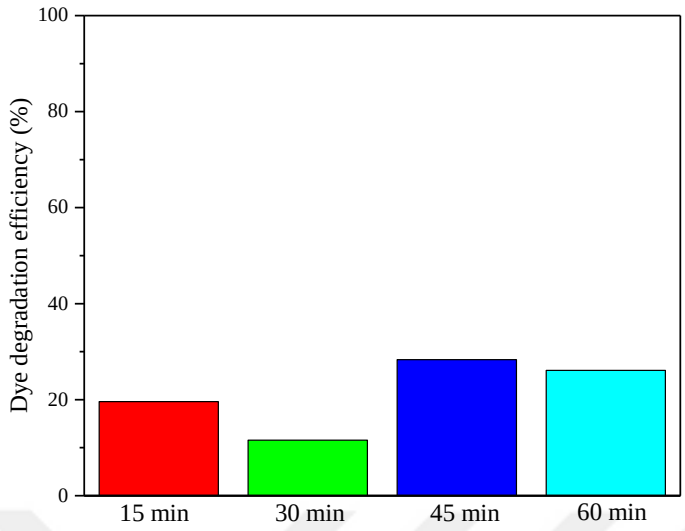

Figure 4.20. Dye degradation efficiencies ZIF-8/TiO_2 composite films with different ZIF-8 growth times

After determining the optimum reaction time for ZIF-8 crystal growth, the ratios of zinc nitrate and methylimidazole in the recipe used in Table 3.2 were changed and the effects of this ratio on the photocatalytic performance of ZIF-8/TiO_2 composite thin film were investigated. The amounts of zinc and methylimidazole were changed, by keeping the amount of methanol constant without making any other changes on the synthesis method. Zinc and Hmim amount decreased to 1/2 (1/2ZIF-8/TiO_2), 1/4 (1/4ZIF-8/TiO_2), 1/8 (1/8ZIF-8/TiO_2) and photocatalytic degradation efficiencies were determined. As seen in Figure 4.21, 1/2ZIF-8/TiO_2, 1/4ZIF-8/TiO_2, 1/8ZIF-8/TiO_2 thin films showed no bigger performance differences that of ZIF-8/TiO_2 composite film. Therefore, the appropriate molar ratio was chosen as 1:8:700 as given in Table 3.2.

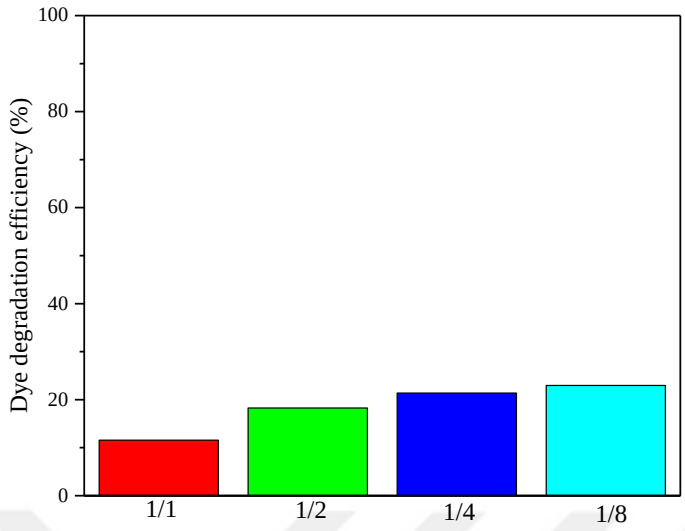

Figure 4.21. Dye degradation efficiencies of 1/1(ZIF-8/TiO_2), 1/2(1/2ZIF-8/TiO_2), 1/4(1/4ZIF-8/TiO_2) and 1/8 (1/8ZIF-8/TiO_2) thin films

ZIF-8 was grown on all pure/doped TiO_2 films and photocatalytic performances were evaluated and compared to that of bare ZIF-8 grown on the glass substrate. TiO_2 thin films which were coated with ZIF-8 were coded with ZT prefix, doped (Ce, Fe, Zn, Cu) TiO_2 thin films which were coated with ZIF-8 were coded as ZTCe, ZTFe, ZTZn and ZTCu. According to Figure 4.22, 1 % ZTCe, 5 % ZTFe, 1 % ZTZn, 1 % ZTCu showed better performance in photocatalytic methylene blue degradation compared to bare ZIF-8.

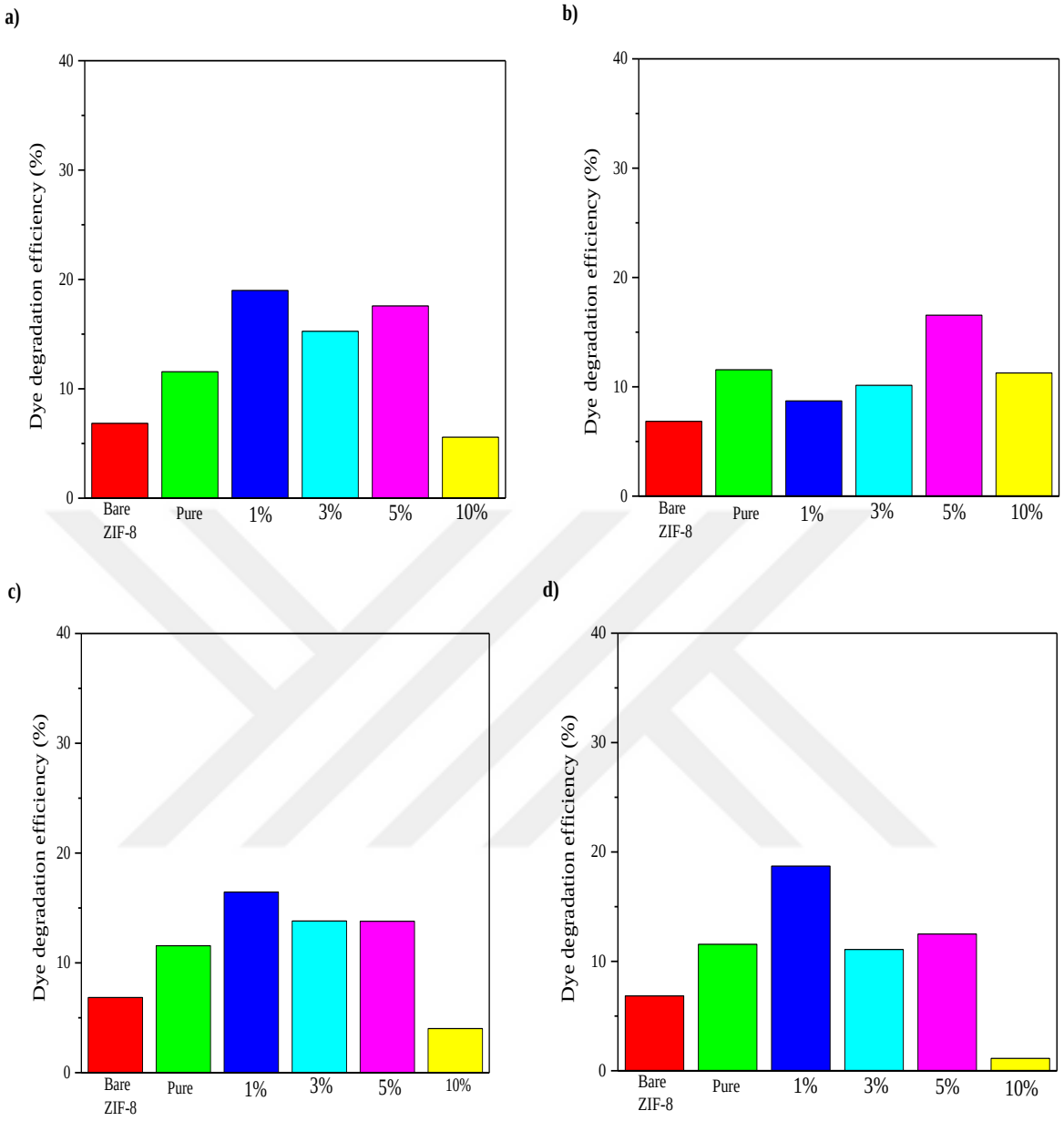

Figure 4.22. Dye degradation efficiencies of a) ZTCe, b) ZTFe, c) ZTZn and d) ZTCu ZIF-8 coated doped TiO_2 thin films after 1 hour

Photocatalytic performances of the prepared films were also evaluated under 365 nm light for prolonged reaction times. ZIF-8/TiO_2 films which showed the highest performances under 254 nm light were chosen. In these experiments, a 365 nm LED lamp was used as the light source and a cooling fan was used to cool the led light. Led and the cooling system was placed on the top of the 11 cm height 10.5 cm sized Plexi box. Thin films were placed on a plastic wafer in a 50 mL beaker and the reaction medium was constantly stirred with a

magnetic bar placed under the films. In these experiments, 2 ppm 20 mL methylene blue was used and experiments were conducted for 4 hours and samples were taken at determined time intervals. According to Figure 4.23, 1 % ZTCe and 1 % ZTCu showed better photocatalytic activities than those of 1 % ZTFe and 1 % ZTZn. All of the composite films showed better activities than bare ZIF-8 indicating that the activity of ZIF-8 was improved when it was grown on TiO_2 substrates.

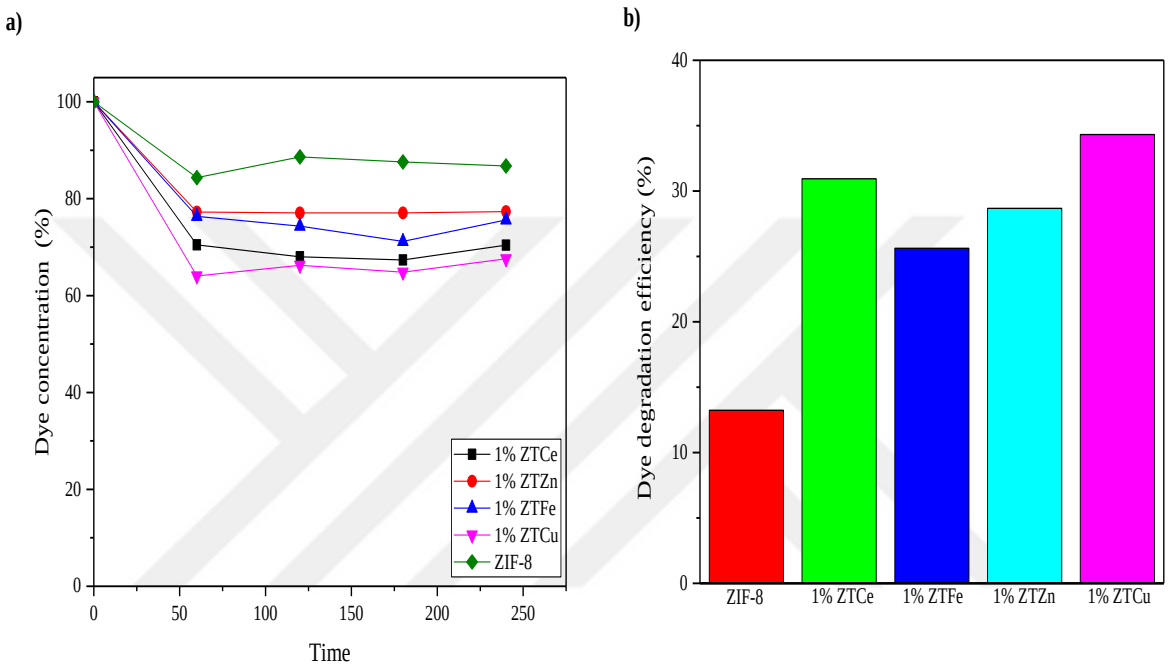

Figure 4.23. a) Time dependent degradation curves and b) dye degradation efficiencies of 1 % ZTCe, 1 % ZTFe, 1 % ZTZn and 1 % ZTCu thin films

4.2.2 Photocatalytic Performances of Particulate Thin Films

Particulate thin films were first prepared by varying coating cycles from 1 to 10. The time-dependent degradation curves and degradation efficiencies of the particulate thin films with the different number of coating layers are given in Figure 4.24. 400°C was chosen for the heat treatment temperature. As can be seen from the figure 4.24 the activity increased with the increasing number of layers up to 5 layers. The activities of 7 and 10 layered films were found to be lower than 5 layered film. Thus, 5 layers was chosen as the optimum number of layers and different heat treatment temperatures were applied to this film.

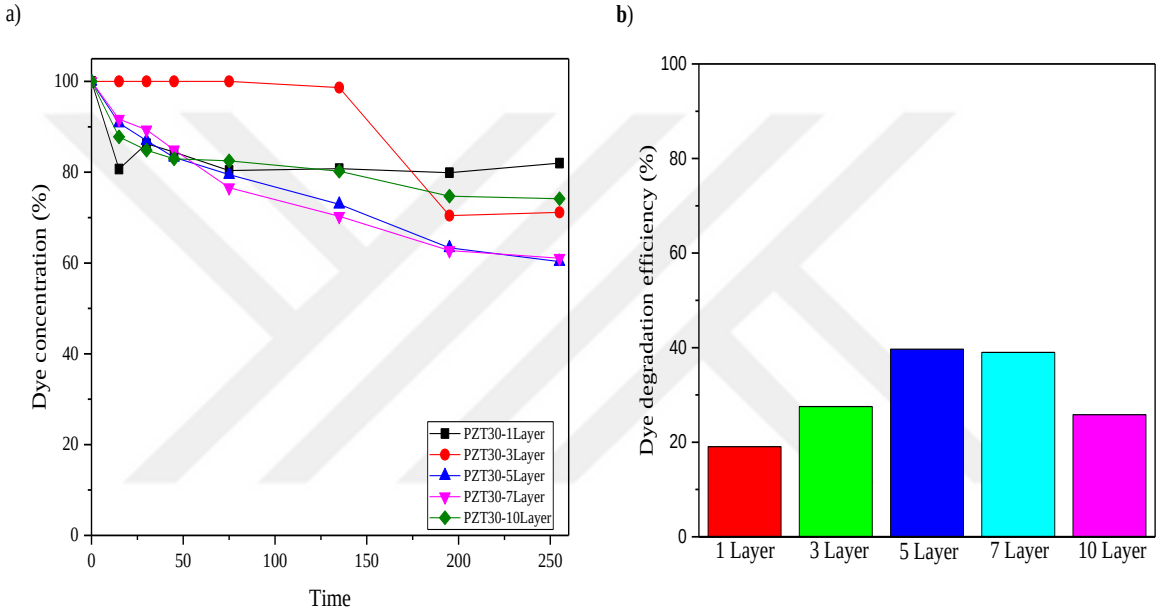

Figure 4.24. a) Time dependent degradation curves and b) dye degradation efficiencies of multi-layered particulate thin films

Time dependent degradation curves and degradation efficiencies of the particulate thin films heat-treated at different temperatures are given in Figure 4.25. The highest efficiency was obtained with the film heat treated at 500°C. According to the light absorption and band gaps of the films, the film heat treated at 500°C has the lowest bandgap which means it can utilize light more efficiently compared to other films. XPS results also showed that ZIF-8 in this film may have been converted to ZnO, thus a heterojunction formed between TiO_2 and ZnO may have increased the activity. Also, an N doped TiO_2 or ZnO may have been formed due to heat treatment which enhanced the photocatalytic activity.

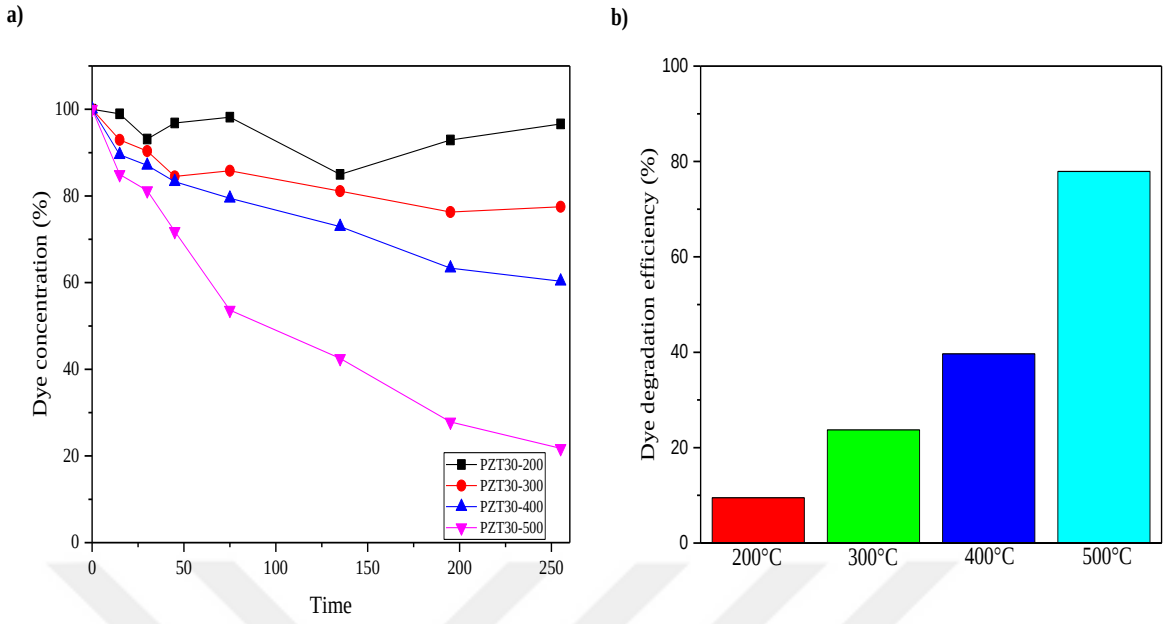

Figure 4.25. a) Time dependent degradation curves and b) dye degradation efficiencies of multi-layered particulate thin films heat treated at different temperatures

Time dependent degradation curves and photocatalytic dye degradation efficiencies of particulate thin films synthesized by using Ag-doped ZIF-8 (PZTAg) or ZIF-L (PZTL) instead of ZIF-8 are shown in Figure 4.26. According to the results, the dye degradation efficiency of PZTAg was found to be 72 % which is slightly lower than the particulate thin film synthesized by ZIF-8. The degradation efficiency of PZTL was found to be 33 % which was very low compared to other films.

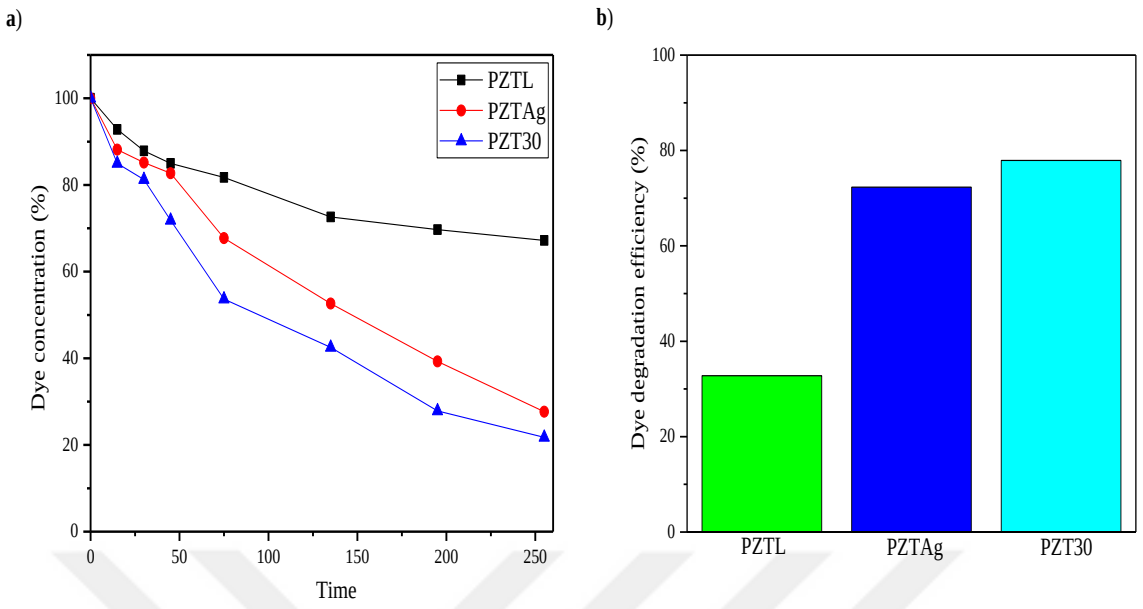

Figure 4.26. a) Time dependent degradation curve b) dye degradation efficiency of PZTL and PZTAg particulate thin films

5. CONCLUSIONS

TiO_2/ZIF-8 based transparent and particulate films were successfully coated on borosilicate glass by the dip-coating method. Performance evaluations of the produced transparent thin films were carried out by methylene blue degradation experiments.

In the first part, the photocatalytic performances of transparent thin films were evaluated. According to the results of ZIF-8/TiO_2 based transparent thin films, methylene blue degradation performance of ZIF-8/TiO_2 thin films prepared by ZIF-8 growth on doped TiO_2 films were higher than bare ZIF-8 thin films grown on borosilicate glass and ZIF-8 films grown on undoped TiO_2 films. Transparent thin films with the highest dye degradation performances were determined to be 1 % ZTCe, 5 % ZTFe, 1 % ZTZn and 1 % ZTCu.

ZIF-8/TiO_2 transparent thin films, 1 % ZTCe, 1 % ZTFe, 1 % ZTZn and 1 % ZTCu which showed high photocatalytic performances under 254 nm light were chosen for methylene blue degradation under 365 nm light. As a result of 4-hour experiments, it was observed that 1 % ZTCe, 1 % ZTFe, 1 % ZTZn and 1 % ZTCu thin films exhibited higher photocatalytic performances than bare ZIF-8. Among the four films, 1 % ZTCe and 1 % ZTCu showed the highest performances.

In the second part the photocatalytic performances of particulate thin films were evaluated. The effects of number of layers and heat treatment temperature on the photocatalytic performance were investigated. The film with 5 layers showed the highest performance among the films with 1, 3, 5, 7 and 10 layered films heat treated at 400°C. 5 layers were determined as the optimum number of layers for the preparation of the particulate thin films. Four different heat treatment temperatures (200, 300, 400 and 500°C) were applied to 5-layered particulate thin films. It was observed that the increase in the heat treatment temperature decreased the band gap energy of the particulate thin films and increased methylene blue degradation performance under 365 nm light. Methylene blue degradation efficiency of the particulate thin film heat treated at 500^{o}C was found to be 78 %. The higher activity of this film was attributed to low band gap energy and the formation of an N doped crystalline ZnO and TiO_2 structure.

Additionally, thin films were prepared by using silver doped ZIF-8 (PZTAg) and ZIF-L crystals (PZTL) instead of ZIF-8 in the production of particulate thin films. The photocatalytic performances of these films were determined under 365 nm light for 4 hours and methylene blue dye degradation efficiencies of PZTAg and PZTL were found to be 72 % and 32 %, respectively, which were lower compared to the films produced by using ZIF-8.

6. RECOMMENDATIONS

The ZIF-8/TiO_2 composite materials have generally been prepared in powder form in scientific literature. However, in this thesis, ZIF-8/TiO_2 composites were produced as transparent and particulate thin films. The results showed that the photocatalytic activity of ZIF-8 can be increased by using ZIF-8 together with TiO_2 in a composite thin film form. The information obtained in this thesis may be a starting point for the production of ZIF-8/TiO_2 thin films which can be used in artificial photosynthesis studies where carbondioxide is reduced to methanol, ethanol and etc.

The photocatalytic activities of the transparent thin films can be increased by varying the number of layers of ZIF-8 and changing the drying conditions such as drying in a vacuum or changing the solvent used in ZIF-8 crystal growth.

The photocatalytic activities of the particulate films can be increased by changing the ratios of ZIF-8, Degussa P25 and TTIP used in the preparation of particulate thin films, by changing the drying conditions after coating or by the addition of dopants such as copper, cerium, iron and zinc into the nanostructure.

REFERENCES

Ahmed, M. A., E.E. El-Katori, and Z.H. Gharni, Photocatalytic degradation of methylene blue dye using Fe_2O_3/TiO_2 nanoparticles prepared by sol–gel method. Journal of Alloys and Compounds, 2013. 553: p. 19-29.

Ajmal, A., et al., Photocatalytic degradation of textile dyes on Cu_2O-CuO/TiO_2 anatase powders. Journal of Environmental Chemical Engineering, 2016. 4(2): p. 2138-2146.

Al-Ghussain, L. (2019). Global warming: review on driving forces and mitigation. *Environmental Progress & Sustainable Energy, 38*(1), 13-21.

Ameta, A. S. (2016). *PHOTOCATALYSIS: Princibles and Application* (1st edition).

Antonia, H. T. E. L., Daniel M. Kammen. (2001). RENEWABLE ENERGY SOURCES. *Encyclopedia of Life Support Systems*.

Arabatzis, I. (2003). Characterization and photocatalytic activity of Au/TiO_2 thin films for azo-dye degradation. *Journal of Catalysis, 220*(1), 127-135.

Barlev, D., Vidu, R., & Stroeve, P. (2011). Innovation in concentrated solar power. *Solar Energy Materials and Solar Cells, 95*(10), 2703-2725.

Barreca, D., et al., Fe_2O_3-TiO_2 Nano-heterostructure Photoanodes for Highly Efficient Solar Water Oxidation. Advanced Materials Interfaces, 2015. 2(17): p. 1500313.

Benramdane, M., Abboudi, S., & Ghernaout, M. (2019). Contribution to the Simulation and Parametric Analysis of the Operation of a Solar Concentration Thermal Installation. *International Journal of Heat and Technology, 37*(2), 446-456.

Cardoso, J. C., Stulp, S., de Brito, J. F., Flor, J. B. S., Frem, R. C. G., & Zanoni, M. V. B. (2018). MOFs based on ZIF-8 deposited on TiO_2 nanotubes increase the surface adsorption of CO_2 and its photoelectrocatalytic reduction to alcohols in aqueous media. *Applied Catalysis B: Environmental, 225*, 563-573.

Chaiko, R. a. Y. (2008). Solar Tracking System: More Efficient Use of Solar Panels. *World Academy of Science, Engineering and Technology, 17*.

Chandra, R., Mukhopadhyay, S., & Nath, M. (2016). TiO_2 @ZIF-8: A novel approach of modifying micro-environment for enhanced photo-catalytic dye degradation and high usability of TiO_2 nanoparticles. *Materials Letters, 164*, 571-574.

Cheng, P., Yang, Z., Wang, H., Cheng, W., Chen, M., Shangguan, W., & Ding, G. (2012). TiO_2–graphene nanocomposites for photocatalytic hydrogen production from splitting water. *International Journal of Hydrogen Energy, 37*(3), 2224-2230.

Chu, Y. (2011). Review and Comparison of Different Solar Energy Technologies. *Global Energy Network Institute (GENI)*.

Dalrymple, O. K. S., EliasTrotz, Maya A.Goswami, D. Yogi. (2010). A review of the mechanisms and modeling of photocatalytic disinfection. *Applied Catalysis B: Environmental, 98*(1-2), 27-38.

Dashtestani, V. M., Leila Maʿmani , Kobra Maafi. (2020). TiO_2 Encapsulated into Zeolitic Imidazolate Framework (TiO_2@ZIF-8) as an Efficient Nanophotocatalyst for Degradation of Paraquat Herbicide. *Journal of Biosafety, 13*.

deKrafft, K. E., C. Wang, and W. Lin, Metal-organic framework templated synthesis of Fe_2O_3/TiO_2 nanocomposite for hydrogen production. Adv Mater, 2012. 24(15): p. 2014-8.

Di Paola, A., Garcia-Lopez, E., Marci, G., & Palmisano, L. (2012). A survey of photocatalytic materials for environmental remediation. *J Hazard Mater, 211-212*, 3-29.

Ediger, V. Ş. (2019). An integrated review and analysis of multi-energy transition from fossil fuels to renewables

ScienceDirect-Energy Procedia, 156, 2-6.
Fazaeli, R., & Aliyan, H. (2018). Novel hierarchical TiO_2@ZIF-8 for photodecolorization of semi-real sample bromothymol blue aqueous solution. *Journal of the Iranian Chemical Society, 16*(1), 1-9.
Feng, S., Zhang, X., Shi, D., & Wang, Z. (2020). Zeolitic imidazolate framework-8 (ZIF-8) for drug delivery: A critical review. *Frontiers of Chemical Science and Engineering, 15*(2), 221-237.
Foster, H. A. D., I. B.Varghese, S.Steele, A. (2011). Photocatalytic disinfection using titanium dioxide: spectrum and mechanism of antimicrobial activity. *Appl Microbiol Biotechnol, 90*(6), 1847-1868.
Fujishima, A. a. K. H., Electrochemical Photolysis of Water at a Semiconductor Electrode. Nature, 1972. 238(5358): p. 37-38.
Gerrity, D. R., H.Crittenden, J. Abbaszadegan, M. (2008). Photocatalytic inactivation of viruses using titanium dioxide nanoparticles and low-pressure UV light. *J Environ Sci Health A Tox Hazard Subst Environ Eng, 43*(11), 1261-1270.
Goetjen, T. A., Liu, J., Wu, Y., Sui, J., Zhang, X., Hupp, J. T., & Farha, O. K. (2020). Metal-organic framework (MOF) materials as polymerization catalysts: a review and recent advances. *Chem Commun (Camb), 56*(72), 10409-10418.
Guo, Y.-F., Fang, W.-J., Fu, J.-R., Wu, Y., Zheng, J., Gao, G.-Q., Wang, C.-C. (2018). Facile synthesis of Ag@ZIF-8 core-shell heterostructure nanowires for improved antibacterial activities. *Applied Surface Science, 435*, 149-155.
Haarindraprasad, R., Hashim, U., Gopinath, S. C., Kashif, M., Veeradasan, P., Balakrishnan, S. R., Poopalan, P. (2015). Low Temperature Annealed Zinc Oxide Nanostructured Thin Film-Based Transducers: Characterization for Sensing Applications. *PLoS One, 10*(7), e0132755.
Hall, J. R. H. (1991). Solid State Physics 131-136.
Hassan, M. E., et al., Heterogeneous photo-Fenton degradation of methyl orange by Fe_2O_3/TiO_2 nanoparticles under visible light. Journal of Water Process Engineering, 2016. 12: p. 52-57.
Houk, B. (1988). Glossary of terms used in photochemistry. *International Union of Pure and Applied Chemistry, 60*, 1055-1106.
Huang, Z., Dong, P., Zhang, Y., Nie, X., Wang, X., & Zhang, X. (2018). A ZIF-8 decorated TiO_2 grid-like film with high CO_2 adsorption for CO_2 photoreduction. *Journal of CO_2 Utilization, 24*, 369-375.
Isimjan, T. T., Kazemian, H., Rohani, S., & Ray, A. K. (2010). Photocatalytic activities of Pt/ZIF-8 loaded highly ordered TiO_2 nanotubes. *Journal of Materials Chemistry, 20*(45), 10241.
Jia, M., Yang, Z., Xu, H., Song, P., Xiong, W., Cao, J., Wang, W. (2020). Integrating N and F co-doped TiO_2 nanotubes with ZIF-8 as photoelectrode for enhanced photo-electrocatalytic degradation of sulfamethazine. *Chemical Engineering Journal, 388*, 124388.
Jing, H.-P., Wang, C.-C., Zhang, Y.-W., Wang, P., & Li, R. (2014). Photocatalytic degradation of methylene blue in ZIF-8. *RSC Adv., 4*(97), 54454-54462.
Kannekanti Lalitha, G. S. a. B. S. M. S., Valluri Durga Kumari,and Neha Y. Hebalkar, Highly Stabilized and Finely Dispersed Cu_2O/TiO_2 : A Promising Visible Sensitive Photocatalyst for Continuous Production of Hydrogen from Glycerol:Water Mixtures, & J. Phys. Chem. C 2010, 22181–22189 2010.
Kazuhito Hahshimoto, H. I. a. A. F. (2005). TiO_2 Photocatalysis: A Historical Overview and Future Prospects. *Japanese Journal of Applied Physics, 44*.

Keidel, E., The fading of aniline dyes in the presence of titanium white. Farben-Zeitung, 1929. 1242–1243.

Khandekar, M. L., Murty, T. S., & Chittibabu, P. (2005). The Global Warming Debate: A Review of the State of Science. *Pure and Applied Geophysics, 162*(8-9), 1557-1586.

Khemthong, P., P. Photai, and N. Grisdanurak, Structural properties of CuO/TiO_2 nanorod in relation to their catalytic activity for simultaneous hydrogen production under solar light. International Journal of Hydrogen Energy, 2013. 38(36): p. 15992-16001.

Koohestani, S.K Sadrnezhaad, Photocatalytic degradation of methyl orange and cyanide by using TiO_2/CuO composite. Desalination and Water Treatment, 2016. 57(46): p. 22029-22038.

Lai, L. S., Yeong, Y. F., Ani, N. C., Lau, K. K., & Shariff, A. M. (2014). Effect of Synthesis Parameters on the Formation of Zeolitic Imidazolate Framework 8 (ZIF-8) Nanoparticles for CO_2 Adsorption. *Particulate Science and Technology, 32*(5), 520-528.

Landau, M. (1913). Le phénomène de la photocatalyse.

Laxma, K., B.Kumar Reddy, P. A.Kim, K. H. (2017). TiO_2-based photocatalytic disinfection of microbes in aqueous media: A review. *Environ Res, 154*, 296-303.

Lee, Y.-R., Jang, M.-S., Cho, H.-Y., Kwon, H.-J., Kim, S., & Ahn, W.-S. (2015). ZIF-8: A comparison of synthesis methods. *Chemical Engineering Journal, 271*, 276-280.

Li, P. Z., Aranishi, K., & Xu, Q. (2012). ZIF-8 immobilized nickel nanoparticles: highly effective catalysts for hydrogen generation from hydrolysis of ammonia borane. *Chem Commun (Camb), 48*(26), 3173-3175.

Li, R., Li, W., Jin, C., He, Q., & Wang, Y. (2020). Fabrication of ZIF-8@TiO_2 micron composite via hydrothermal method with enhanced absorption and photocatalytic activities in tetracycline degradation. *Journal of Alloys and Compounds, 825*, 154008.

Liu, J., et al., Photocatalytic conversion of nitrogen to ammonia with water on triphase interfaces of hydrophilic-hydrophobic composite $Bi_4O_5Br_2$/ZIF-8. Chemical Engineering Journal, 2019. 371: p. 796-803.

Liu, Y., et al., Photostable core-shell CdS/ZIF-8 composite for enhanced photocatalytic reduction of CO_2. Applied Surface Science, 2019. 498: p. 143899.

Luanwuthi, S., Krittayavathananon, A., Srimuk, P., & Sawangphruk, M. (2015). In situ synthesis of permselective zeolitic imidazolate framework-8/graphene oxide composites: rotating disk electrode and Langmuir adsorption isotherm. *RSC Advances, 5*(58), 46617-46623.

Madras, T. Aarthi (2007). Photocatalytic Degradation of Rhodamine Dyes with Nano-TiO_2. *Ind. Eng. Chem. Res, 46*, 7-14.

Mahmoodi, N. M., & Abdi, J. (2019). Nanoporous metal-organic framework (MOF-199): Synthesis, characterization and photocatalytic degradation of Basic Blue 41. *Microchemical Journal, 144*, 436-442.

Mahmoodi, N. M., et al., Metal-organic framework (ZIF-8)/inorganic nanofiber (Fe_2O_3) nanocomposite: Green synthesis and photocatalytic degradation using LED irradiation. Journal of Molecular Liquids, 2019. 291: p. 111333.

Miensah, E., Chen, J., Gu, A., Wang, P., Liu, Y., Gong, C., Yang, Y. Sonicated Zeolitic Imidazolate Frameork-8 derived Nitrogen-doped hierarchical nanoporous carbon for e (2021).

Moises A Carreon, S. R. V. (2020). Metal-Organic Framework Membranes for Molecular Gas Separations. *Wold Scientific, 6*, 284.

Munoz-Gil, D., & Figueiredo, F. M. L. (2019). High Surface Proton Conduction in Nanostructured ZIF-8. *Nanomaterials (Basel), 9*(10).

Nakano, R. I., H.Yao, Y.Kajioka, J.Fujishima, A.Sunada, K.Minoshima, M.Hashimoto, K.Kubota, Y. (2012). Photocatalytic inactivation of influenza virus by titanium dioxide thin film. *Photochem Photobiol Sci, 11*(8), 1293-1298.

Ni, M., Leung, M. K. H., Leung, D. Y. C., & Sumathy, K. (2007). A review and recent developments in photocatalytic water-splitting using TiO_2 for hydrogen production. *Renewable and Sustainable Energy Reviews, 11*(3), 401-425.

Oi, L. E., Choo, M.-Y., Lee, H. V., Ong, H. C., Hamid, S. B. A., & Juan, J. C. (2016). Recent advances of titanium dioxide (TiO_2) for green organic synthesis. *RSC Advances, 6*(110), 108741-108754.

Owusu, P. A., Asumadu-Sarkodie, S., & Dubey, S. (2016). A review of renewable energy sources, sustainability issues and climate change mitigation. *Cogent Engineering, 3*(1), 1167990.

Panchal, H. S., Kishor K. Essa, Fadl A. Shanmugan, Sengottain Sathyamurthy, Ravishankar. (2020). Enhancement of the yield of solar still with the use of solar pond: A review. *Heat Transfer, 50*(2), 1392-1409.

Panwara, S. C. K., Surendra Kotharia, & (2011). Role of renewable energy sources in environmental protection: A review. *Renewable and Sustainable Energy Reviews, 15*(3), 1513-1524.

Perez, R. P. M. (2009). A Fundamental Look At Energy Reserves for the Planet. *Shc Solar Update*.

Periyat, P., Naufal, B., & Ullattil, S. G. (2016). A Review on High Temperature Stable Anatase TiO_2 Photocatalysts. *Materials Science Forum, 855*, 78-93.

Pipelzadeh, E., Rudolph, V., Hanson, G., Noble, C., & Wang, L. (2017). Photoreduction of CO_2 on ZIF-8/TiO_2 nanocomposites in a gaseous photoreactor under pressure swing. *Applied Catalysis B: Environmental, 218*, 672-678.

Qi, X., Shang, F., Wang, T., Ma, Y., & Yan, Y. (2020). In situ coupling of TiO_2(B) and ZIF-8 with enhanced photocatalytic activity via effective defect. *CrystEngComm, 22*(25), 4250-4259.

Qiu, J., et al., Constructing Cd0.5Zn0.5S@ZIF-8 nanocomposites through self-assembly strategy to enhance Cr(VI) photocatalytic reduction. J Hazard Mater, 2018. 349: p. 234-241.

Ramesh Chandra, V. S., Shailly Tomar & Mala Nath. (2019). Multi-core-shell composite SnO_2NPs@ZIF-8: potential antiviral agent and effective photocatalyst for waste-water treatment.

Ren, Koshy, P., Chen, W. F., Qi, S., & Sorrell, C. C. (2017). Photocatalytic materials and technologies for air purification. *J Hazard Mater, 325*, 340-366.

Ren, J., Langmi, H. W., North, B. C., & Mathe, M. (2015). Review on processing of metal-organic framework (MOF) materials towards system integration for hydrogen storage. *International Journal of Energy Research, 39*(5), 607-620.

Rincón, A.-G., & Pulgarin, C. (2004). Field solar E. coli inactivation in the absence and presence of TiO_2: is UV solar dose an appropriate parameter for standardization of water solar disinfection? *Solar Energy, 77*(5), 635-648.

Rochkind, M. P., S. Paz, Y. (2014). Using dyes for evaluating photocatalytic properties: a critical review. *Molecules, 20*(1), 88-110.

Sanjinés, R., Tang, H., Berger, H., Gozzo, F., Margaritondo, G., & Lévy, F. (1994). Electronic structure of anatase TiO_2 oxide. *Journal of Applied Physics, 75*(6), 2945-2951.

Sheng, L., Yang, F., Wang, C., Yu, J., Zhang, L., & Pan, Y. (2017). Comparison of the hydrothermal stability of ZIF-8 nanocrystals and polycrystalline membranes derived from zinc salt variations. *Materials Letters, 197*, 184-187.

Shi, Y., Yang, A.-F., Cao, C.-S., & Zhao, B. (2019). Applications of MOFs: Recent advances in photocatalytic hydrogen production from water. *Coordination Chemistry Reviews, 390*, 50-75.

Shibli, S. M. A. a. J. N. S., Development of Fe_2O_3–TiO_2 mixed oxide incorporated Ni–P coating for electrocatalytic hydrogen evolution reaction. International Journal of Hydrogen Energy, 2013. 38(5): p. 2271-2282.

Sun, X., Wang, C., Su, D., Wang, G., & Zhong, Y. (2020). Application of Photocatalytic Materials in Sensors. *Advanced Materials Technologies, 5*(5), 1900993.

Teng, F., et al., Effect of TiO_2 Surface Structure on the Hydrogen Production Activity of the Pt@CuO/TiO_2 Photocatalysts for Water Splitting. ChemCatChem, 2014. 6(3): p. 842-847.

Tran,., et al., Novel of TiO_2/Ag_3PO_4/Bentonite Composite Photocatalyst: Preparation, Characterization, and Application for Degradation of Methylene Blue in Aqueous Solution. Environmental Engineering Science, 2019. 36(1): p. 71-80.

Wang, H.-T., et al., Design and synthesis of porous C–ZnO/TiO_2@ZIF-8 multi-component nano-system via pyrolysis strategy with high adsorption capacity and visible light photocatalytic activity. Microporous and Mesoporous Materials, 2019. 288: p. 109548.

Wei, X., et al., Composite ZIF-8 with CQDs for boosting visible-light-driven photocatalytic removal of NO. Journal of Alloys and Compounds, 2019. 802: p. 467-476.

Wu, N. (2004). Enhanced TiO_2 photocatalysis by Cu in hydrogen production from aqueous methanol solution. *International Journal of Hydrogen Energy, 29*(15), 1601-1605.

Yilin Xu, X. L., Yuqing Lin,Chandresh Maldec,Rong Wang. (2019). Synthesis of ZIF-8 based composite hollow fiber membrane with a dense skin layer for facilitated biogas upgrading in gas-liquid membrane contactor.

Yoong, L. S., Chong, F. K., & Dutta, B. K. (2009). Development of copper-doped TiO_2 photocatalyst for hydrogen production under visible light. *Energy, 34*(10), 1652-1661.

YU You-Yi Reduced Graphene Oxide Coupled Magnetic $CuFe_2O_4$-TiO_2 Nanoparticles with Enhanced Photocatalytic Activity for Methylene Blue Degradation. *Chinese Journal of Structural Chemistry*, 2016. Vol.35.

Zeng, M., Chai, Z., Deng, X., Li, Q., Feng, S., Wang, J., & Xu, D. (2016). Core–shell CdS@ZIF-8 structures for improved selectivity in photocatalytic H2 generation from formic acid. *Nano Research, 9*(9), 2729-2734.

Zhan, Y., Lan, J., Shang, J., Yang, L., Guan, X., Li, W., Lin, S. (2020). Durable ZIF-8/Ag/AgCl/TiO_2 decorated PAN nanofibers with high visible light photocatalytic and antibacterial activities for degradation of dyes. *Journal of Alloys and Compounds, 822*, 153579.

Zhang, Zhou, P., Liu, J., & Yu, J. (2014). New understanding of the difference of photocatalytic activity among anatase, rutile and brookite TiO_2. *Phys Chem Chem Phys, 16*(38), 20382-20386.

Zhang, L., Yi,Shuai, Danmeng,Shen, Yun,Wang, Dawei. (2019). Progress and challenges in photocatalytic disinfection of waterborne Viruses: A review to fill current knowledge gaps. *Chemical Engineering Journal, 355*, 399-415.

Zhang, M., Shang, Q., Wan, Y., Cheng, Q., Liao, G., & Pan, Z. (2019). Self-template synthesis of double-shell TiO_2@ZIF-8 hollow nanospheres via sonocrystallization

with enhanced photocatalytic activities in hydrogen generation. *Applied Catalysis B: Environmental, 241*, 149-158.

Zhong, W.-L., Li, C., Liu, X.-M., Bai, X.-K., Zhang, G.-S., & Lei, C.-X. (2020). Liquid phase deposition of flower-like TiO_2 microspheres decorated by ZIF-8 nanoparticles with enhanced photocatalytic activity. *Microporous and Mesoporous Materials, 306*, 110401.

Zhou, L., Zhang, H., Sun, H., Liu, S., Tade, M. O., Wang, S., & Jin, W. (2016). Recent advances in non-metal modification of graphitic carbon nitride for photocatalysis: a historic review. *Catalysis Science & Technology, 6*(19), 7002-7023.

Zhu, S., et al., Fe_2O_3/TiO_2 photocatalyst of hierarchical structure for H2 production from water under visible light irradiation. Microporous and Mesoporous Materials, 2014. 190: p. 10-16.